NASA TN D-416

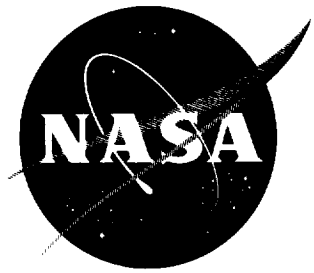

TECHNICAL NOTE
D-416

ANALYTICAL INVESTIGATION OF THE DYNAMIC BEHAVIOR OF A NONLIFTING MANNED REENTRY VEHICLE

By Jacob H. Lichtenstein

Langley Research Center
Langley Field, Va.

NATIONAL AERONAUTICS AND SPACE ADMINISTRATION

WASHINGTON

September 1960

NATIONAL AERONAUTICS AND SPACE ADMINISTRATION

TECHNICAL NOTE D-416

ANALYTICAL INVESTIGATION OF THE DYNAMIC BEHAVIOR OF A NONLIFTING MANNED REENTRY VEHICLE

By Jacob H. Lichtenstein

SUMMARY

An analytic investigation was made of the dynamic behavior of a nonlifting manned reentry vehicle as it descended through the atmosphere. The investigation included the effects of variations in the aerodynamic stability derivatives, the spin rate, reentry angle, and velocity. The effect of geostrophic winds and of employing a drogue parachute for stability purposes were also investigated.

It was found that for the portion of the flight above a Mach number of 1 a moderate amount of negative damping could be tolerated but below a Mach number of 1 good damping is necessary. The low-speed stability could be improved by employing a drogue parachute. The effectiveness of the drogue parachute was increased when attached around the periphery of the rear of the vehicle rather than at the center. Neither moderate amounts of spin or the geostrophic winds had appreciable effects on the stability of the vehicle. The geostrophic winds and the reentry angle or velocity all showed important effects on the range covered by the reentry flight path.

INTRODUCTION

There is, at present, considerable interest in the dynamics of bodies entering the earth's atmosphere. This interest stems from the concern about the behavior of both satellite (manned or unmanned) and ballistic missiles as they descend through the atmosphere. As a result of this interest numerous papers have been published by the NASA and others, some of which discuss the trajectory of reentry bodies (for instance, refs. 1 to 4) and some of which discuss the dynamic stability of the reentry body as well (for instance, refs. 5 to 12).

The present paper reports the results of an analytic investigation into the dynamic behavior of a representative nonlifting manned satellite as it descends through the atmosphere. This investigation encompassed the effects of changes of the aerodynamic derivatives and rate of spin

on the stability of the vehicle. Computations were made to assess the advantages of using a drogue parachute to enhance the subsonic stability of an otherwise marginal or unstable body. In this connection the relative merits of attaching the parachute towline at one central point or at several points around the periphery at the rear of the body were also investigated. In addition, the effects of the earth's spin and of variations in the angle of entry and initial velocity were computed. The computations for this program were made on an IBM 704 electronic data processing machine.

SYMBOLS

The axes system used in the present program is shown in figure 1.

A maximum cross-sectional area, sq ft

a radial distance from center line of body to parachute attachment point on body, ft

a^* value of a used as step input at some specified value of $\frac{v - V_Y}{V_R}$ with the sign of a varying as the sign of $\frac{v - V_Y}{V_R}$ (see appendix A)

a^{**} value of a used as step input at some specified value of $\frac{w - V_Z}{V_R}$ with the sign of a varying as the sign of $\frac{w - V_Z}{V_R}$ (see appendix A)

C_D drag coefficient

$C_m = \frac{\text{Pitching moment}}{QAd}$

C_{m_α} variation of pitching-moment coefficient with angle of attack in XZ-plane, $\frac{\partial C_m}{\partial \alpha_Z}$, per radian

C_{m_q} damping-in-pitch coefficient, $\frac{\partial C_m}{\partial\left(\frac{qd}{2V_R}\right)}$

$C_n = \frac{\text{Yawing moment}}{QAd}$

C_{n_α} variation of yawing-moment coefficient with angle of attack in XY-plane, $\frac{\partial C_n}{\partial \alpha_Y}$, per radian

C_{n_r} damping-in-yaw coefficient, $\frac{\partial C_n}{\partial\left(\frac{rd}{2V_R}\right)}$

$C_X = \frac{\text{Axial force}}{QA}$

$C_{X,p} = \frac{\text{Axial force of drogue parachute}}{QA}$

$C_Y = \frac{\text{Side force}}{QA}$

C_{Y_r} variation of side-force coefficient with nondimensional yawing velocity, $\frac{\partial C_Y}{\partial\left(\frac{rd}{2V_R}\right)}$

C_{Y_α} rate of change of side-force coefficient with angle of attack in XY-plane, $\frac{\partial C_Y}{\partial \alpha_Y}$, per radian

$C_Z = \frac{\text{Normal force}}{QA}$

C_{Z_α} rate of change of normal-force coefficient with angle of attack in XZ-plane, $\frac{\partial C_Z}{\partial \alpha_Z}$, per radian

C_{Z_q} variation of normal-force coefficient with nondimensional pitching velocity, $\frac{\partial C_Z}{\partial\left(\frac{qd}{2V_R}\right)}$

d	maximum body diameter, ft
F	force, lb
F_g	force due to gravity, lb
F_X, F_Y	forces along X- and Y-axes, respectively, lb
g	acceleration due to gravity at surface of earth, ft/sec^2
h	altitude above surface of earth, $R - R_e$, ft
I	moment of inertia, $slug\text{-}ft^2$
I_X	moment of inertia about X-axis, $slug\text{-}ft^2$
I_Y, I_Z	moment of inertia about Y- and Z-axes (same value), respectively, $slug\text{-}ft^2$
K	damping factor, $-2C_X + C_{Z_\alpha} + \left(C_{m_q} + C_{m_{\dot{\alpha}}}\right)\frac{d^2m}{2I_Y}$
l	distance rearward from body center of gravity to drogue-parachute attachment point on body, ft (see sketch in appendix B)
M	moment about center of gravity
M_X, M_Y, M_Z	moments about X-, Y-, and Z-axes, respectively, ft-lb
m	mass, slugs
N_{Ma}	Mach number, $\frac{V_R}{\text{Speed of sound}}$
n	acceleration along flight path, $\frac{\Delta V}{g\Delta t}$, g units
p,q,r	angular velocities about X-, Y-, and Z-axes, respectively, radians/sec
Q	dynamic pressure, $\frac{1}{2}\rho V_R^2$, lb/sq ft

$\frac{qd}{2V_R}$	nondimensional pitching-velocity parameter referred to diameter
R	radial distance from origin of the X_i-, Y_i-, and Z_i-axes system to origin of X-, Y-, and Z-axes system, ft
R_e	radius of earth, taken as 21×10^6, ft
$\frac{rd}{2V_R}$	nondimensional yawing-velocity parameter referred to diameter
u,v,w	components of velocity along X-, Y-, and Z-axes, respectively, ft/sec
V	resultant inertial velocity of vehicle, $\sqrt{u^2 + v^2 + w^2}$, ft/sec
V_R	resultant velocity of vehicle with respect to air, ft/sec
V_X,V_Y,V_Z	components of geostrophic wind along X-, Y-, and Z-axes, respectively, ft/sec
X,Y,Z	reference axes with origin at center of mass of body with X-axis alined along line of symmetry
X_i,Y_i,Z_i	inertial reference axes with origin at center of earth
x,y,z	distance from origin along X_i-, Y_i-, and Z_i-axes to center of gravity of vehicle
α	total angle of attack, deg
α_Y	angle of attack in XY-plane, deg
α_Z	angle of attack in XZ-plane, deg
γ	flight-path angle, deg
θ,ψ,ϕ	Euler angles defined in figure 1, radians
$\bar{\theta}$	angle between X_iZ_i-plane and location vector to vehicle (latitude)
ρ	density of air (standard atmosphere tables for density variation with altitude, from Rocket Panel Proposal of April 1955), slugs/cu ft

σ radius of gyration $\sqrt{\frac{I}{M}}$, sq ft

$\bar{\psi}$ angle in X_iZ_i-plane between X_iY_i-plane and plane containing vehicle (west longitude)

Ω rate of spin of the earth, taken as 0.000073 radian/sec

Subscripts:

max maximum

min minimum

o indicates initial value

p indicates drogue parachute

A dot over a symbol indicates differentiation with respect to time.

CALCULATIONS

Computations were made of the motion of a body representative of a manned satellite upon its reentry into and descent through the earth's atmosphere. The computations were made on an IBM 704 electronic data processing machine and the conditions for the computations are given in table I. The dimensional and mass characteristics of the vehicle are given in table II. The general reentry configuration considered for the study is shown in figure 2 and the methods of drogue-parachute attachment are shown in figure 3. For the two-point attachment with $a/d = 0.3125$ the parachute lines are attached at the periphery of the rear face. For the two-point attachment with $a/d = 0.625$ the parachute lines are attached to arms extending outward from the surface at the rear. The equations of motion used in these calculations are given in appendix A and the development of the terms used to simulate the drogue parachute are given in appendix B.

For a computation of this type where the frequency of oscillation varies through very wide limits $\left(\text{Frequency} \approx \sqrt{Q}\right)$, a constant computing interval which would insure repeatability at the high frequencies would be very wasteful at the lower frequencies. Therefore, a program in which the number of points per oscillation cycle was prescribed was used rather than a fixed time interval. It was found that computing between 20 and 40 points per cycle generally was sufficient for adequate repeatability.

The following general pattern was used in making the computations: From reentry at an altitude of 380,000 feet down to an altitude where $N_{Ma} = 1$, the aerodynamic derivatives were considered constant and the drogue-parachute terms were considered zero; below a Mach number of 1 some aerodynamic derivatives were changed to values that were more representative of low-speed values, and the drogue-parachute terms were included. Thus, it was possible to compute for the low-speed part of the run the various effects of aerodynamic derivatives and drogue-parachute configuration without the necessity of recomputing any of the high-speed part of the run. The mass characteristics and stability derivatives used were the most representative of the desired configurations that were available at the time the computations were made. Some computations were made with the mass characteristics shown for condition 1 (see table II) which were early estimates. These values were changed to those listed for condition 2 when these more representative data became available; however, it was not deemed worthwhile to recompute the earlier runs.

RESULTS AND DISCUSSION

Presentation of Results

The results of this investigation are presented in figures 4 to 14 according to the arrangement shown in table I. The data divide conveniently into two parts: the high-speed portion, from reentry down to the altitude where $N_{Ma} = 1$, and the low-speed portion, below $N_{Ma} = 1$ where the drogue parachute generally was employed. The data for the high-speed portion are presented in figures 4 to 9. The results of the low-speed portion of the trajectory, including the effects of employing a drogue parachute for stability, are shown in figures 10 to 14. Generally, these computations were made starting with the point at $N_{Ma} = 1$ for the basic condition (run 1, table I).

Basic Condition

The data for the basic condition are given in figure 4. This condition is listed as run 1 in table I and the aerodynamic derivatives that were used are $C_{m_q} = 0.37$, $C_{m_\alpha} = -0.20$, and $C_{Z_\alpha} = -0.28$ for Mach numbers greater than 1 and $C_{m_q} = -1.00$, $C_{m_\alpha} = -0.05$, and $C_{Z_\alpha} = 0.60$ for Mach numbers less than 1. At the time the computations were made these values of the derivatives were considered those most representative of the configuration. For a condition with no spin there is no disturbance in the yaw plane and therefore the motion is confined to the pitch plane

only. The variations of dynamic pressure Q, of deceleration along the flight path n, of Mach number N_{Ma}, and of the envelope of the angle-of-attack oscillation α with altitude are shown in figure 4(a). The variations of Q, n, and N_{Ma} are typical of those for most of the runs and therefore are not presented for the rest of the runs. The variation of altitude with range is shown in figure 4(b); this variation also is typical of the trajectories for most of the cases. It should be mentioned that since this is a plot of altitude against range the true curvature of the flight path in inertial space is not shown. In order to obtain the true curvature, a plot of x against y would be needed.

At the beginning of the reentry trajectory, 380,000 feet, the dynamic pressure was so low that an aerodynamic moment sufficiently large to turn the vehicle along the curvature of the flight path was not generated, and consequently the angle of attack increased from the initial 1° up to 1.6° at 374,000 feet. At this point the pitching moment became large enough to turn the vehicle along the flight path and an oscillation in angle of attack developed. The first few cycles of the oscillation are shown in the angle-of-attack envelope plot in figure 4(a). The increasing dynamic pressure as the vehicle descended through the atmosphere had a constraining effect on the amplitude of the oscillation. The fact that a minimum value of α occurs before the maximum value of Q occurs is due to the destabilizing effects of axial force and negative damping. Below the point of maximum Q the angle-of-attack amplitude expands rapidly until $N_{Ma} = 1$. Below $N_{Ma} = 1$ the positive aerodynamic damping rapidly decreases the amplitude.

Effect of Aerodynamic Derivatives on Amplitude Envelope of Angle of Attack Above a Mach Number of 1

The effect of changes in the damping derivative C_{m_q}, the normal-force-curve slope C_{Z_α}, and the static stability parameter C_{m_α} are shown in figure 5. Varying the damping coefficient from $C_{m_q} = 0.37$ to $C_{m_q} = -0.90$ (fig. 5(a)) decreased the amplitude of the angle-of-attack oscillation as would be expected. This effect is confined to the lower portion of the trajectory where the decreasing dynamic pressure permits the effect of the aerodynamic damping to develop. During the upper portion of the trajectory the confining effect of increasing dynamic pressure was predominant and little effect of aerodynamic damping is seen. A dynamic stability factor defined in reference 8 is given by $K = \left[-2C_X + C_{Z_\alpha} + \frac{1}{2}\left(C_{m_q} + C_{m_{\dot{\alpha}}}\right)\left(\frac{d}{\sigma}\right)^2\right]$. This parameter varied from 4.04 for $C_{m_q} = 0.37$ to -0.14 for $C_{m_q} = -0.90$ (table I)

indicating a change from strong instability to slight stability. It is interesting to note that only for the case where the dynamic stability factor is negative does the amplitude of the angle-of-attack oscillation continuously decrease from reentry down to the altitude where $N_{Ma} = 1$.

The damping contributed by the normal-force-curve slope C_{Z_α} is illustrated by the comparison shown in figure 5(b). For the case where the damping coefficient C_{m_q} was zero, it can be seen that a negative value of C_{Z_α} corresponding to a positive lift-curve slope has a stabilizing effect.

The effect of changes in the static stability parameter C_{m_α} on the angle-of-attack envelope is shown in figure 5(c) and on the frequency of oscillation in figure 6. For the basic configuration the maximum frequency of oscillation was about 0.9 cycle per second at maximum dynamic pressure. The values of C_{m_α} were altered sufficiently to decrease the maximum frequency to 1/4 cycle per second in one case $\left(C_{m_\alpha} = -0.016\right)$ and increase the frequency to 4 cycles per second in the other $\left(C_{m_\alpha} = -4.000\right)$. For the lower frequency case $\left(C_{m_\alpha} = -0.016\right)$ a considerably larger amplitude of oscillation was obtained throughout the trajectory; this was a result of the behavior at the early stage of the trajectory. Because of the considerably smaller value of C_{m_α} for this case the angle of attack built up to almost 3.5° compared with 1.6° for the basic condition before the vehicle was able to develop a sufficient moment to follow the flight path. For the case in which the frequency of oscillation was higher the vehicle almost immediately starts to follow the flight path with the consequently smaller amplitude of oscillation throughout the run. The computations for this high-frequency case were stopped at about 170,000 feet because the high frequency of oscillation required that a very large number of data points be computed in order to define adequately the oscillation. This would consume an unusually great amount of computing time and the additional information to be obtained was not considered worth the machine effort required. In addition to the variation of frequency with altitude obtained from the complete computations, the frequency obtained from the simple relationship $\text{Frequency} = \frac{1}{2\pi}\sqrt{\frac{QAdC_{m_\alpha}}{I}}$ is shown in figure 6. The agreement between the two methods is very good, which indicates that if the dynamic pressure is known the simple computations would give an adequate representation of the frequency of oscillation.

Effect of Rate of Spin

The effect of constant rate of spin about the vehicle longitudinal axis on the angle-of-attack envelope is shown in figure 7. The motion of the vehicle for the spinning case is not an oscillation in the normal sense as it is for the nonspinning case but a precessional type of motion; the double curves in figure 7 indicate the maximum and minimum angles of attack during the precessing motion. The fact that the maximum and the minimum angles of attack are so nearly the same indicates that the precession is nearly circular about the flight path. The data show that for a spin rate of 1 rpm, which is considered sufficient to nullify the dispersion due to configuration asymmetry, the maximum angle of attack, which occurs at the Mach number of 1, is only slightly larger (about 2°) than that obtained for the nonspinning case. Increasing the spin rate had a deleterious effect on the angle-of-attack amplitude in that for a spin rate of 19.1 rpm the angle-of-attack amplitude exceeded 80° and for a spin rate of 57.3 rpm it exceeded 90°. These large angles of attack result mainly from the increased stiffness of the spinning body relative to the normal aerodynamic moment tending to turn the body into the flight path. Because of this increased resistance to turning and the low aerodynamic moments during the early part of the trajectory, the spinning vehicle tended to remain in its initial attitude considerably longer than did the nonspinning vehicle; therefore, the spinning vehicle built up to a larger value of angle of attack. Thereafter, the effect of dynamic pressure and damping were similar to that obtained for the nonspinning case. The fact that the ratio of the maximum angle-of-attack amplitude obtained at $N_{Ma} = 1$ to the minimum angle-of-attack amplitude is about the same for the spinning and nonspinning cases ($\alpha_{max}/\alpha_{min} = 20$ for the nonspinning case, 20 for the 1-rpm case, and 23 for the 19.1-rpm case) indicates that the instability obtained near Mach number 1 is attributable mainly to the factors discussed in the previous sections.

L
8
6
7

Effect of Earth Spin

The effects of including the geostrophic winds (winds due to the earth's spin) on the angle-of-attack envelope and trajectories are shown in figure 8. The data in figure 8(a) show that the geostrophic winds in the form of head or tail winds have a negligible effect on the stability of the vehicle. For the crosswind case (vehicle traveling north, perpendicular to earth's spin) the angle-of-attack pattern is similar but approximately twice as large as it is for the other cases. In this instance the geostrophic wind adds an appreciable angle in the yaw plane to the angle already present in the pitch plane, whereas for the other cases the geostrophic wind merely alters the relative wind by about $5\frac{1}{2}$ percent. There is, however, an appreciable effect on the location

of the impact point for all three cases. The trajectories in figure 8(b) show that for a reentry in the same direction as the earth's spin (going east) there is a tail wind and the vehicle travels farther than for the nonspinning case (basic condition). A point on the surface of the earth directly under the point of reentry will move in the same direction as the vehicle because of the earth's spin and thus the apparent range will be decreased. During the time the vehicle is descending, the point on the surface actually moves farther than the increase in range caused by the geographic tail wind, and, therefore, the net range is less for a body reentering in the same direction as the earth spin than it would be for a stationary earth. (See the following table.) For a body reentering against the earth's spin exactly the opposite is true.

L
8
6
7

Direction of reentry	Vehicle total travel, miles	Travel of a point on surface of earth, miles	Net vehicle travel, miles
East (with earth spin)	2,102	206	1,896
No spin	1,989	0	1,989
West (against earth spin)	1,884	202	2,086

For a vehicle heading north at reentry the basic trajectory is not appreciably affected by introducing earth spin (1,989 miles). The vehicle, however, drifts in an easterly direction 76 miles during its flight because of geostrophic winds. A point on the surface originally at the same longitude as the reentry point but at the latitude at which impact takes place will have moved eastward 180 miles. The net effect, therefore, is such that the vehicle appears to move westward 104 miles.

Effect of Reentry Angle and Velocity

The basic initial velocity for most of the computations was 25,752 ft/sec which is the orbital velocity for a body in a 380,000-foot circular orbit. The data in figure 9 show the effect of increasing the angle of reentry from 0° to 3° for the same initial velocity and at a 1° angle of attack. The data in figure 10 show the effect of decreasing this initial velocity up to 10 percent for a reentry angle of 0°. The effect on the range traversed from initiation of the reentry to the point of impact was much the same for both variables in that there was a very rapid decrease in range for the initial 1° declination or the initial 2-percent reduction in velocity. Thereafter, the relative change in the range was much smaller.

Although all these runs started with an initial angle of attack of 1° they exhibited an increase in angle of attack at the start of the trajectory because the dynamic pressure developed at this high altitude was insufficient to turn the vehicle along the flight path (figs. 9(c) and 10(b)). Once sufficient dynamic pressure has been developed, however, the angle-of-attack envelope pattern is similar for all the runs, and the difference in magnitude depends upon the magnitude of the angle of attack attained at the beginning of the run.

Effects of Single-Point-Attachment Drogue Parachute, of C_{m_q}, and of C_{Z_α} on Angle-of-Attack Envelope at Low Speeds

The effect of the damping coefficient C_{m_q} for both the clean vehicle and the vehicle with a single-point-attachment drogue parachute is presented in figure 11. The beneficial effect of having good aerodynamic damping is immediately apparent. If the damping is good $\left(C_{m_q} = -0.5 \text{ or better}\right)$ the drogue parachute helps very little, If, on the other hand, the damping is low the drogue parachute will contribute materially to reducing the amplitude of oscillation. Changing the value of C_{Z_α} from a destabilizing value of 0.6 to a stabilizing value of -0.28 produces an appreciable improvement when the damping is low and, as noted before, this type of change has only minor effect when good damping exists (fig. 12).

In addition to this damping effect, the drogue parachute increases the frequency of oscillation by a factor of 3. At an altitude of 72,000 feet the frequency of oscillation increased from 0.20 cps without the drogue parachute to 0.61 cps with the drogue parachute.

Effect of Two-Point Attachment of Drogue Parachute

The effectiveness of the various methods of drogue-parachute attachment to the vehicle in decreasing the amplitude of the angle-of-attack oscillation for the case of $C_{m_q} = 0$ is shown in figure 13. The progressive benefits of going from no parachute to a single-point-attachment parachute then to the two-point-attachment of the parachute for $\frac{a}{d} = 0.3125$ and for $\frac{a}{d} = 0.625$ are quite obvious. In the practical case the two-point-attachment methods mentioned would be at least four-point-attachment systems (two in the pitch plane and two in the yaw plane). Each of the various parachute-attachment methods seems to act as a limiter on the amplitude of the oscillation.

Besides having an appreciable effect on the angle-of-attack amplitude the drogue parachutes have a marked effect on the frequency of the oscillation. This effect is shown in the following table where the frequencies for the various methods of parachute attachment are given for an altitude of 72,000 feet, which is just below the altitude at which they are initially employed:

Type of attachment	Frequency obtained from IBM data, cps	Frequency obtained from one-degree-of-freedom computation, cps
No parachute	0.20	0.21
Single point	.61	.61
Two point, a/d = 0.3125	1.36	1.36
Two point, a/d = 0.625	1.86	1.85

The increase in the frequency of oscillation as the configuration is changed from one with no parachute to one with an extended two-point $\left(\frac{a}{d} = 0.625\right)$ attachment is obvious. The table also shows that the frequency can be adequately predicted by making a one-degree-of-freedom computation of the time history of the angle of attack using the Laplace transform method so that the initial conditions for the offcenter parachute attachment can be included.

The effect of using a two-point attachment $\left(\frac{a}{d} = 0.3125\right)$ instead of a single-point attachment for several damping coefficients $\left(C_{m_q} = 0, -0.5, \text{ and } -1.0\right)$ is shown in figure 14. It can be seen that for each damping coefficient the use of the two-point attachment instead of the single-point attachment resulted in an improvement in the angle-of-attack envelope. For high values of C_{m_q} of course, the improvement is not nearly so great as it is for low values of damping. Computations for the two-point-attachment $\frac{a}{d} = 0.625$, cases with large values of damping were not made because it was believed that the large improvement shown for $C_{m_q} = 0$ (fig. 13) indicated that there would be a progressive improvement for the larger damping values and that the machine time could be better utilized for other aspects of the problem.

Drogue-Parachute Effects at Large Angles of Attack

In order to investigate the effects of the drogue parachute opening at angles of attack other than a value of 5° (already discussed) computations were made for several cases in which the initial conditions were similar to those for the parachute opening at the original 5° angle of attack but with the angle of attack arbitrarily increased to 10°, 20°, 40°, and 60°. It should be mentioned here that these computations are, strictly, not applicable for the large angles considered because the stability derivatives used were assumed to be constant with angle of attack and because, for the development of the drogue-parachute terms, the analysis was limited to small angles of attack. However, the results should be useful for indicating the gross effects of the drogue-parachute behavior. The data for these computations are presented in figure 15; it can be seen that for zero damping coefficient the drogue parachute attached at a single point can only effect enough damping to maintain the initial angle of 60°. This result is in agreement with the data presented in figure 11 where it was shown that for zero damping coefficient the drogue parachute permitted the angle of attack to build up to a limiting value of about 60°. For a higher damping coefficient of $C_{m_q} = -0.5$ it can be seen that the angle-of-attack envelope was damped quite well and also that the damping was nonlinear, being greater at the large angles than it was at the smaller angles. In order to show this effect somewhat clearer, three curves are shown for each of the initial angles of attack of 60° and 40° in figure 15(b). One curve is the curve obtained for the normal 5° amplitude case multiplied by factors of 8 or 12 in order to give initial angles of 40° and 60°, respectively. The second curve is one in which the drogue-parachute term is omitted from that portion of the equations where it is multiplied by $qd/2V_R$ in the Y-moment equation and $rd/2V_R$ in the Z-moment equation. It was included in all the other parts of the equation. (See appendix A.) The third curve is the same as that presented in figure 15(a) which was obtained by using the full equations. It can be seen that the parachute is effective in introducing damping even though those terms that would normally be associated with a damping coefficient have been omitted and that when these terms are included there is a considerable increase in damping. The difference between the expanded 5° curve and the normal computations is a measure of the nonlinearity of the damping at these higher angles.

The effect of the drogue parachute attached at two points at these higher angles of attack is shown in figure 15(c) for an initial amplitude of 60° and in figure 15(d) for an initial amplitude of 40°. It can be seen that going progressively from a single-point attachment to a two-point attachment $\left(\frac{a}{d} = 0.3125 \text{ then } \frac{a}{d} = 0.625\right)$ made substantial increases in the damping of the angle-of-attack envelope. As a matter

L 8 6 7

of fact, for the $\frac{a}{d} = 0.625$ two-point attachment the damping was satisfactory even for $C_{m_q} = 0$ (fig. 15(c)). The data in figure 15(d) for 40° initial amplitude indicate a very similar pattern to that for 60° initial amplitude and will not be discussed further.

CONCLUSIONS

An analytical study of the dynamic behavior of a typical manned nonlifting reentry vehicle has indicated the following conclusions:

1. In the high-speed portion of the trajectory (above a Mach number of 1) a moderate amount of negative damping can be tolerated without too adverse an effect on the angle-of-attack oscillation. Below a Mach number of 1, however, reasonably good damping is necessary $\left(C_{m_q} = -0.5\right)$ in order to avoid divergence of the angle of attack.

2. The stability can be improved, at low speeds, by employing a drogue parachute. The effectiveness of the drogue parachute is progressively increased as the attachment is changed from a single point on the longitudinal axis to several points around the periphery of the rear face and then to outrigger arms extending outward from the surface at the rear.

3. A moderate rate of spin, enough to remove dispersion caused by vehicle asymmetry (about 1 rpm), would not have a serious adverse effect on the vehicle stability. Higher rates of spin, however, would be deleterious.

4. Geostrophic winds did not have a serious effect on the vehicle stability; they did, however, appreciably alter the impact point.

5. Increasing the reentry angle or decreasing the initial velocity from basic orbital conditions had a similar effect on the range in that a small change in either the angle (1°) or velocity (2 percent) at first effected a large decrease in range but thereafter similar changes had considerably smaller effects.

Langley Research Center,
National Aeronautics and Space Administration,
Langley Field, Va., April 11, 1960.

APPENDIX A

EQUATIONS OF MOTION

The equations of motion used in this investigation are for a modified body axes system (fig. 1). The axes system differs from the usual body axes system in that the Z-axis is constrained to remain in a plane parallel to the X_iZ_i inertial plane and in that the body is free to spin about the X body axis. The X-axis is always alined with the axis of symmetry of the body. These equations are in a form frequently employed in ballistics work, and they may be derived by resolving equations of motion in a normal body axis system into the XYZ modified body axis system as shown in reference 11. Therefore, a full development of the equations will not be presented. The equations used herein are as follows:

L 8 6 7

X-force equation:

$$\dot{u} = \frac{QA}{m}\left(C_X' + C_{X,p}'\right) + rv - qw$$

$$-g\frac{R_e^2}{R^3}(x\cos\psi\cos\theta + y\sin\theta + z\sin\psi\cos\theta)$$

where $C_X' = C_X\cos\alpha$ and $C_{X,p}' = C_{X,p}\cos\alpha$.

Y-force equation:

$$\dot{v} = \frac{QA}{m}\left(\left(C_{Y_\alpha} + C_{X,p}\right)\left(\frac{v - V_Y}{V_R}\right) + \left\{C_{Y_r} - 4C_{X,p}\left[\frac{l}{d}\left(\frac{v - V_Y}{V_R}\right)^2 + \frac{a^*}{d}\left(\frac{v - V_Y}{V_R}\right)\right]\right\}\frac{rd}{2V_R}\right)$$

$$- ru + qw\tan\theta - g\frac{R_e^2}{R^3}(-x\cos\psi\sin\theta + y\cos\theta - z\sin\psi\sin\theta)$$

Z-force equation:

$$\dot{w} = \frac{QA}{m}\left(\left(C_{Z_\alpha} + C_{X,p}\right)\left(\frac{w - V_Z}{V_R}\right) + \left\{C_{Z_q} + 4C_{X,p}\left[\frac{l}{d}\left(\frac{w - V_Z}{V_R}\right)^2 + \frac{a^{**}}{d}\left(\frac{w - V_Z}{V_R}\right)\right]\right\}\frac{qd}{2V_R}\right)$$

$$+ qu - qv\tan\theta - g\frac{R_e^2}{R^3}(-x\sin\psi + z\cos\psi)$$

Y-moment equation:

$$\dot{q} = \frac{QAd}{I_Y}\left(\left(C_{m_\alpha} + C_{X,p}\,\frac{l}{d}\right)\left(\frac{w - V_Z}{V_R}\right) + C_{X,p}\,\frac{a^{**}}{d} + \left\{C_{m_q} + 4C_{X,p}\left[\left(\frac{l}{d}\right)^2\left(\frac{w - V_Z}{V_R}\right)^2 + 2\,\frac{la^{**}}{d^2}\left(\frac{w - V_Z}{V_R}\right) + \left(\frac{a^{**}}{d}\right)^2\right]\right\}\frac{qd}{2V_R}\right) - \frac{I_X}{I_Y}\,pr + rq\tan\theta$$

L
8
6
7

Z-moment equation:

$$\dot{r} = \frac{QAd}{I_Y}\left(\left(C_{n_\alpha} - C_{X,p}\,\frac{l}{d}\right)\left(\frac{v - V_Y}{V_R}\right) - C_{X,p}\,\frac{a^{*}}{d} + \left\{C_{n_r} + 4C_{X,p}\left[\left(\frac{l}{d}\right)^2\left(\frac{v - V_Y}{V_R}\right)^2 + \frac{2la^{*}}{d^2}\left(\frac{v - V_Y}{V_R}\right) + \left(\frac{a^{*}}{d}\right)^2\right]\right\}\frac{rd}{2V_R}\right) + \frac{I_X}{I_Y}\,pq - q^2\tan\theta$$

where

$$\alpha = \arcsin\frac{\sqrt{(v - V_Y)^2 + (w - V_Z)^2}}{V_R}$$

$$V_R = \sqrt{(u - V_X)^2 + (v - V_Y)^2 - (w - V_Z)^2}$$

$$\dot{\phi} = p - q\tan\theta$$

$$\dot{\theta} = r$$

$$\dot{\psi} = -q/\cos\theta$$

and

$$\dot{x} = u \cos\theta \cos\psi - v \sin\theta \cos\psi - w \sin\psi$$

$$\dot{y} = u \sin\theta + v \cos\theta$$

$$\dot{z} = u \cos\theta \sin\psi - v \sin\theta \sin\psi + w \cos\psi$$

$$V_X = \Omega R_e \cos\bar{\theta}\left[\cos\left(\frac{\pi}{2} - \bar{\psi}\right)\cos\psi \cos\theta - \sin\left(\frac{\pi}{2} - \bar{\psi}\right)\sin\psi \cos\theta\right]$$

$$V_Y = \Omega R_e \cos\bar{\theta}\left[-\cos\left(\frac{\pi}{2} - \bar{\psi}\right)\cos\psi \sin\theta + \sin\left(\frac{\pi}{2} - \bar{\psi}\right)\sin\psi \sin\theta\right]$$

$$V_Z = \Omega R_e \cos\bar{\theta}\left[-\cos\left(\frac{\pi}{2} - \bar{\psi}\right)\sin\psi - \sin\left(\frac{\pi}{2} - \bar{\psi}\right)\cos\psi\right]$$

$$\bar{\theta} = \arctan\frac{y}{\sqrt{x^2 + z^2}}$$

$$\left(\frac{\pi}{2} - \bar{\psi}\right) = \arctan\frac{x}{z}$$

Range in equatorial plane = $R_e\left(\frac{\pi}{2} - \bar{\psi}\right)$

Range in meridian plane = $R_e(\bar{\theta})$

APPENDIX B

DEVELOPMENT OF TERMS USED TO SIMULATE DROGUE PARACHUTE IN EQUATIONS OF MOTION

The terms used to simulate the drogue parachute in the equations of motion are developed in this appendix. In order to simplify the equations it is assumed that the line attaching the parachute to the vehicle is long relative to the magnitude of the displacement of the attachment point; therefore the drag force acts straight back in line with the relative wind, and any motion of the parachute is omitted. In addition, higher order terms which would considerably complicate the computations but add little to the effects investigated are omitted.

The drogue parachute thus provides pure drag force and the forces and moments along the body axes are provided by the angular displacement of the body and the motion of the attachment point about the center of gravity of the body.

The force applied to the vehicle by the drogue parachute is given by

$$F_p = Q_p A_p C_{D,p}$$

and the moment is given by

$$M_p = Q_p A_p C_{D,p} k_p$$

where k_p is the moment arm of the parachute force. The dynamic pressure Q_p acting on the parachute is

$$Q_p = \frac{1}{2}\rho V_p^2$$

By referring to the following sketch

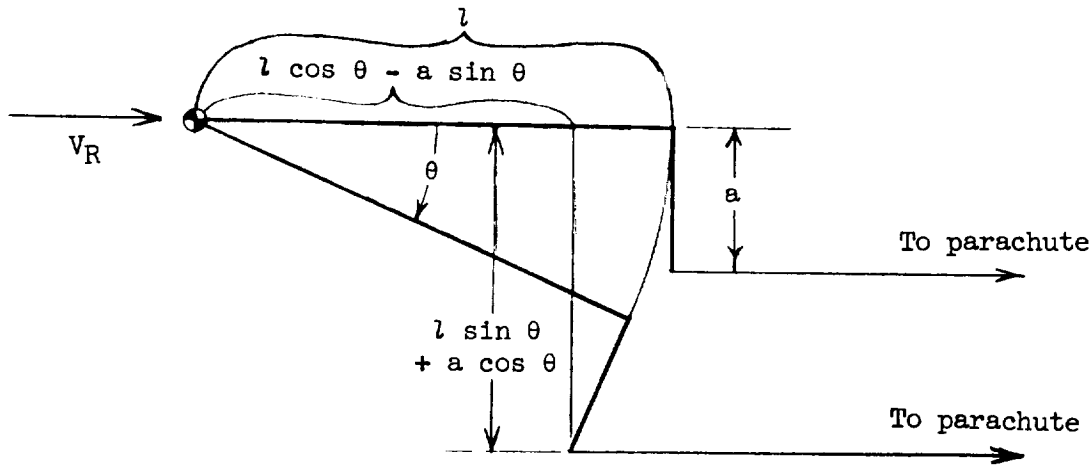

L
8
6
7

it can be seen that

$$V_p = V_R + \Delta V = V_R + l\dot{\theta} \sin \theta + a\dot{\theta} \cos \theta$$

and

$$V_p^2 = V_R^2 + 2V_R(l\dot{\theta} \sin \theta + a\dot{\theta} \cos \theta) + l^2\dot{\theta}^2\sin^2\theta$$

$$+ 2al\dot{\theta}^2 \sin \theta \cos \theta + a^2\dot{\theta}^2\cos^2\theta$$

Assume angles small enough so that $\sin \theta \approx \theta$ and $\cos \theta \approx 1$. The equation for V_p^2 thus reduces to

$$V_p^2 = V_R^2 + 2V_R\dot{\theta}(l\theta + a) + \dot{\theta}^2\left(l^2\theta^2 + 2al\theta + a^2\right)$$

The dynamic pressure becomes

$$Q_p = \frac{1}{2}\rho V_R^2\left[1 + 4\,\frac{\dot{\theta}d}{2V_R}\left(\frac{l}{d}\,\theta + \frac{a}{d}\right) + 4\,\frac{\dot{\theta}^2d^2}{4V_R^2}\left(\frac{l^2\theta^2}{d^2} + 2\,\frac{al}{d^2}\,\theta + \frac{a^2}{d^2}\right)\right]$$

The term $\frac{\dot{\theta}d}{2V_R}$ is a small fraction and therefore it is believed that omission of the terms containing $\left(\frac{\dot{\theta}d}{2V_R}\right)^2$ would not affect the results

appreciably. Thus, the equation for the dynamic pressure can be written as

$$Q_p = \frac{1}{2}\rho V_R^2\left[1 + 4\,\frac{\dot{\theta}d}{2V_R}\left(\frac{l}{d}\,\theta + \frac{a}{d}\right)\right]$$

The term k_p of the moment equation is $k_p = l \sin\theta + a\cos\theta \approx l\theta + a$. The equation for the force now becomes

$$F_p = QA_pC_{D,p}\left[1 + 4\,\frac{\dot{\theta}d}{2V_R}\left(\frac{l}{d}\,\theta + \frac{a}{d}\right)\right]$$

and the equation for the moment becomes

$$M_p = QA_pC_{D,p}\left[l\theta + a + 4\,\frac{\dot{\theta}d}{2V_R}\left(\frac{l^2}{d}\,\theta^2 + 2\,\frac{al}{d}\,\theta + \frac{a^2}{d}\right)\right]$$

The forces and moments due to the offcenter attachment points of the drogue-parachute lines (the terms containing a) require some further explanation. As the vehicle oscillates from positive to negative angles of attack first one parachute line will be taut and the other slack; then, they will reverse. The taut line bears the full load whereas the slack line has no load. Therefore, at the angle of attack where the lines change from slack to taut there will be an immediate shift in load from one side to the other and the load will not be proportional to the angle of attack. Thus, it can be recognized that this term is a step function which changes sign with the angle of attack.

The force and moment coefficients to be used in the equations can now be determined.

X-force coefficients: For this force the second and third terms in the force equations $\left(\text{those containing the term } \frac{\dot{\theta}d}{2V_o}\right)$ are small compared with 1 and can therefore be neglected and the equation for the incremental force along the X-axis due to the parachute reduces to

$$\Delta F_X = QA\,\Delta C_X = -QA_pC_{D,p}$$

and for ΔC_X the following expression is obtained:

$$\Delta C_X = - \frac{QA_p C_{D,p}}{QA}$$

Let $\frac{A_p}{A} C_{D,p} = -C_{X,p}$. Thus,

$$\Delta C_X = C_{X,p}$$

L
8
6
7

Y-force coefficients: The equation for the incremental force along the Y-axis due to the parachute is

$$\Delta F_Y = QA\, \Delta C_Y = QA_p C_{D,p} \left[1 + 4 \frac{\dot{\theta} d}{2V_R} \left(\frac{l}{d} \theta + \frac{a}{d} \right) \right] \theta$$

and

$$\Delta C_Y = -C_{X,p} \left[\theta + 4 \frac{\dot{\theta} d}{2V_R} \left(\frac{l}{d} \theta^2 + \frac{a}{d} \theta \right) \right]$$

The coefficient can be broken up into two terms, a term ΔC_{Y_α} proportional to α and a term ΔC_{Y_r} proportional to $\frac{\dot{\theta} d}{2V_R}$. Taking into account the proper signs for the axes system used gives the following expression for ΔC_{Y_α}

$$\Delta C_{Y_\alpha} = C_{X,p}$$

and the term ΔC_{Y_r} becomes

$$\Delta C_{Y_r} = -4 C_{X,p} \left[\frac{l}{d} \left(\frac{v - V_Y}{V_R} \right)^2 + \frac{a}{d} \left(\frac{v - V_Y}{V_R} \right) \right]$$

Z-force coefficients: In a manner similar to that used to obtain ΔC_Y it can be shown that the terms in the Z-force equation are

$$\Delta C_{Z_\alpha} = C_{X,p}$$

and

$$\Delta C_{Z_q} = 4C_{X,p}\left[\frac{l}{d}\left(\frac{w - V_Z}{V_R}\right)^2 + \frac{a}{d}\left(\frac{w - V_Z}{V_R}\right)\right]$$

Y-moment coefficients: The incremental moment about the Y-axis due to the parachute is

$$\Delta M_Y = -QAd\,\Delta C_m = -QA_pC_{D,p}\left[l\theta + a + 4\,\frac{\dot{\theta}d}{2V_o}\left(\frac{l^2}{d}\,\theta^2 + 2\,\frac{al}{d}\,\theta + \frac{a^2}{d}\right)\right]$$

and the incremental coefficient becomes

$$\Delta C_m = C_{X,p}\left[\frac{l}{d}\,\theta + \frac{a}{d} + 4\,\frac{\dot{\theta}d}{2V_R}\left(\frac{l^2}{d^2}\,\theta^2 + 2\,\frac{al}{d^2}\,\theta + \frac{a^2}{d^2}\right)\right]$$

Here, as for the forces, the total coefficient can be broken up into sections so that when proper cognizance of signs is made the coefficients become

$$\Delta C_{m_\alpha} = C_{X,p}\,\frac{l}{d}$$

$$\Delta C_{m_q} = 4C_{X,p}\left[\frac{l^2}{d^2}\left(\frac{w - V_Z}{V_R}\right)^2 + 2\,\frac{la}{d^2}\left(\frac{w - V_Z}{V_R}\right) + \frac{a^2}{d^2}\right]$$

and

$$\Delta C_m = C_{X,p}\,\frac{a}{d}$$

Z-moment coefficient: In a manner similar to that used to obtain the Y-moment coefficients it can be shown that

$$\Delta C_{n_\alpha} = -C_{X,p} \frac{l}{d}$$

$$\Delta C_{n_r} = 4C_{X,p}\left[\frac{l^2}{d^2}\left(\frac{v - V_Y}{V_R}\right)^2 + 2\,\frac{la}{d^2}\left(\frac{v - V_Y}{V_R}\right) + \frac{a^2}{d^2}\right]$$

$$\Delta C_n = -C_{X,p} \frac{a}{d}$$

REFERENCES

1. Allen, H. Julian, and Eggers, A. J., Jr.: A Study of the Motion and Aerodynamic Heating of Ballistic Missiles Entering the Earth's Atmosphere at High Supersonic Speeds. NACA Rep. 1381, 1958. (Supersedes NACA TN 4047.)

2. Chapman, Dean R.: An Approximate Analytical Method for Studying Entry Into Planetary Atmospheres. NACA TN 4276, 1958.

L
8
6
7 3. Nielsen, Jack N., Goodwin, Frederick K., Mersman, William A.: Three-Dimensional Orbits of Earth Satellites, Including Effects of Earth Oblateness and Atmospheric Rotation. NASA MEMO 12-4-58A, 1958.

4. Eggers, Alfred J., Jr., Allen, H. Julian, and Neice, Stanford E.: A Comparative Analysis of the Performance of Long-Range Hypervelocity Vehicles. NACA Rep. 1382, 1958. (Supersedes NACA TN 4046.)

5. Friedrich, Hans R., and Dore, Frank J.: The Dynamic Motion of a Missile Descending Through the Atmosphere. Jour. Aero. Sci., vol. 22, no. 9, Sept. 1955, pp. 628-632, 638.

6. Charters, A. C.: The Linearized Equations of Motion Underlying the Dynamic Stability of Aircraft, Spinning Projectiles, and Symmetrical Missiles. NACA TN 3350, 1955.

7. Nicolaides, John D.: On the Free Flight Motion of Missiles Having Slight Configurational Asymmetries. Rep. No. 858, Ballistic Res. Labs., Aberdeen Proving Ground, June 1953.

8. Allen, H. Julian: Motion of a Ballistic Missile Angularly Misalined With the Flight Path Upon Entering the Atmosphere and Its Effect Upon Aerodynamic Heating, Aerodynamic Loads, and Miss Distance. NACA TN 4048, 1957.

9. Tobak, Murray, and Allen, H. Julian: Dynamic Stability of Vehicles Traversing Ascending or Descending Paths Through the Atmosphere. NACA TN 4275, 1958.

10. Sommer, Simon C., and Tobak, Murray: Study of the Oscillatory Motion of Manned Vehicles Entering the Earth's Atmosphere. NASA MEMO 3-2-59A, 1959.

11. Bird, John D., and Llewellyn, Charles P.: An Analysis of the Stability of Spinning Disks During Atmospheric Reentry. NASA TM X-248, 1960.

12. Bird, John D., and Wolhart, Walter D.: An Analysis of the Stability and Control of Ballistic Supersonic Impact Reentry Bodies. NASA TM X-198, 1960.

TABLE I.- CALCULATIONS

[For all computations C_{Y_r} and C_{Z_q} were zero and the initial conditions were: $x_o = 0$, $y_o = 0$, $z_o = 21{,}380{,}000$ feet, $q_o = 0$, and $r_o = 0$]

Run	Mass condition	C_X	$C_{X,p}$	C_{Z_α} and C_{Y_α}	C_{m_α} and $-C_{n_\alpha}$	C_{m_q} and C_{n_r}	V_o, ft/sec	γ_o, deg	α_o, deg	p_o, radian/sec	Ω, radian/sec	Plane of entry	Figure -	K	$\frac{a}{d}$	Effect of -
1	II	-1.55 ($N_{Ma} > 1$) -.93 ($N_{Ma} < 1$)	0 ($N_{Ma} > 1$) -.403 ($N_{Ma} < 1$)	-0.28 ($N_{Ma} > 1$) .60 ($N_{Ma} < 1$)	-0.20 ($N_{Ma} > 1$) -.05 ($N_{Ma} < 1$)	0.37 ($N_{Ma} > 1$) -1.00 ($N_{Ma} < 1$)	25,752	-1	1	0	0	Equatorial	4	4.04	0	Basic condition
2					-0.20	0 ($N_{Ma} > 1$)							5	2.82		C_{m_q} and C_{Z_α}
3						-0.37 ($N_{Ma} > 1$)								1.60		C_{m_q} and C_{Z_α}
4						-0.9 ($N_{Ma} > 1$)								-0.14		C_{m_q} and C_{Z_α}
5				0		0 ($N_{Ma} > 1$)								3.10		C_{m_q} and C_{Z_α}
6				-0.28 ($N_{Ma} > 1$) .60 ($N_{Ma} < 1$)	-0.016	-0.37 ($N_{Ma} > 1$)							5 and 6	4.04		C_{m_α}
7					-4.00								5			C_{m_α}
8					-0.20 ($N_{Ma} > 1$) -.05 ($N_{Ma} < 1$)	-0.37 ($N_{Ma} > 1$) -1.0 ($N_{Ma} < 1$)				0.11			7			Rate of spin
9										2.0						Rate of spin
10										6.0						Rate of spin
11										0	0.000073		8			Geostrophic winds
12											-0.000073					Geostrophic winds
13											0.000073	Meridian				Geostrophic winds
14	I					0 ($N_{Ma} > 1$) -1.0 ($N_{Ma} < 1$)		0			0	Equatorial	9	2.82		Initial reentry angle
15								-1								Initial reentry angle
16								-2								Initial reentry angle
17								-3								Initial reentry angle
18							25,494	0					10			Variation of initial entry velocity
19							25,237									Variation of initial entry velocity
20							24,464									Variation of initial entry velocity
21							23,177									Variation of initial entry velocity

TABLE I.- CALCULATIONS - Concluded

Run	Mass condition	C_X	$C_{X,p}$	C_{Z_α} and C_{Y_α}	C_{m_α} and $-C_{n_\alpha}$	C_{m_q} and C_{n_r}	V_0, ft/sec	γ_0, deg	α_0, deg	p_0, radian/sec	q, radian/sec	Plane of entry	Figure -	K	$\frac{a}{d}$	Effect of -
22	● II	-0.93 ($N_{Ma} < 1$)	0	0.60	-0.05	0	[a]980.09	[a]-75.22	[a]5	0	0	Equa-torial	11		0	C_{m_q} and single-point-attachment drogue parachute
23						-0.5										
24						-1.0										
25			-0.405			0										
26						-0.5										
27						-1.0										
28				-0.28		0							12			C_{Z_α} for two values of C_{m_q} with drogue parachute
29						-1.0										
30				0.60		● 0							13		0.3125	Type of drogue parachute attachment and C_{m_q}
31						0									0.625	
32						0.5							14		0.3125	
33						-1.0										
34						-0.5			10				15(a)		0	Initial amplitude of oscillation on drogue parachute performance
35									20							
36									40							
37									60							
38						0			60							
39			-0.405 for drag; 0 for damping equations			-0.5			40				15(b)			Drogue parachute on damping at large angles of attack
40									60							
41			-0.405			0			60				15(c)		0.3125	Type of drogue parachute attachment on damping at large angles of attack
42						-0.5										
43						0									0.625	
44						-0.5										
45									40				15(d)		0.3125	
46															0.625	

[a]Values at $N_{Ma} = 1$ for run 1.

TABLE II.- MASS AND DIMENSIONAL DATA

	Condition I	Condition II
m, slugs	53.2	65.22
I_X, slug-ft^2	448	280
I_Y, slug-ft^2	473	440
A, sq ft	34.91	34.91
d, ft	6.667	6.667
l/d	1.0125	1.0125
a/d		0.3125 and 0.6250
$\frac{W}{C_D S}$ (above M = 1)	31.66	38.81

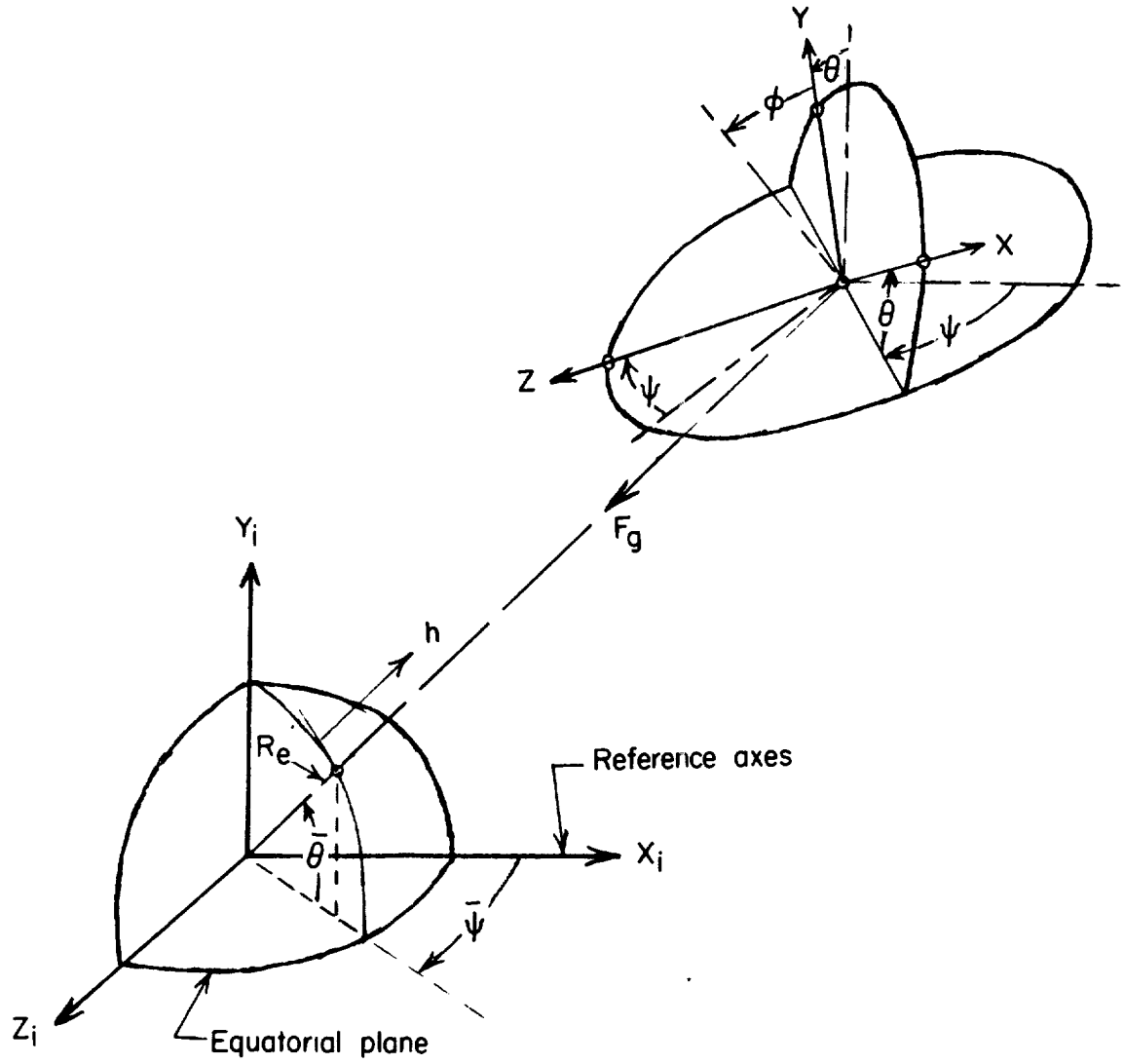

I-867

Figure 1.- Axes system used in computations.

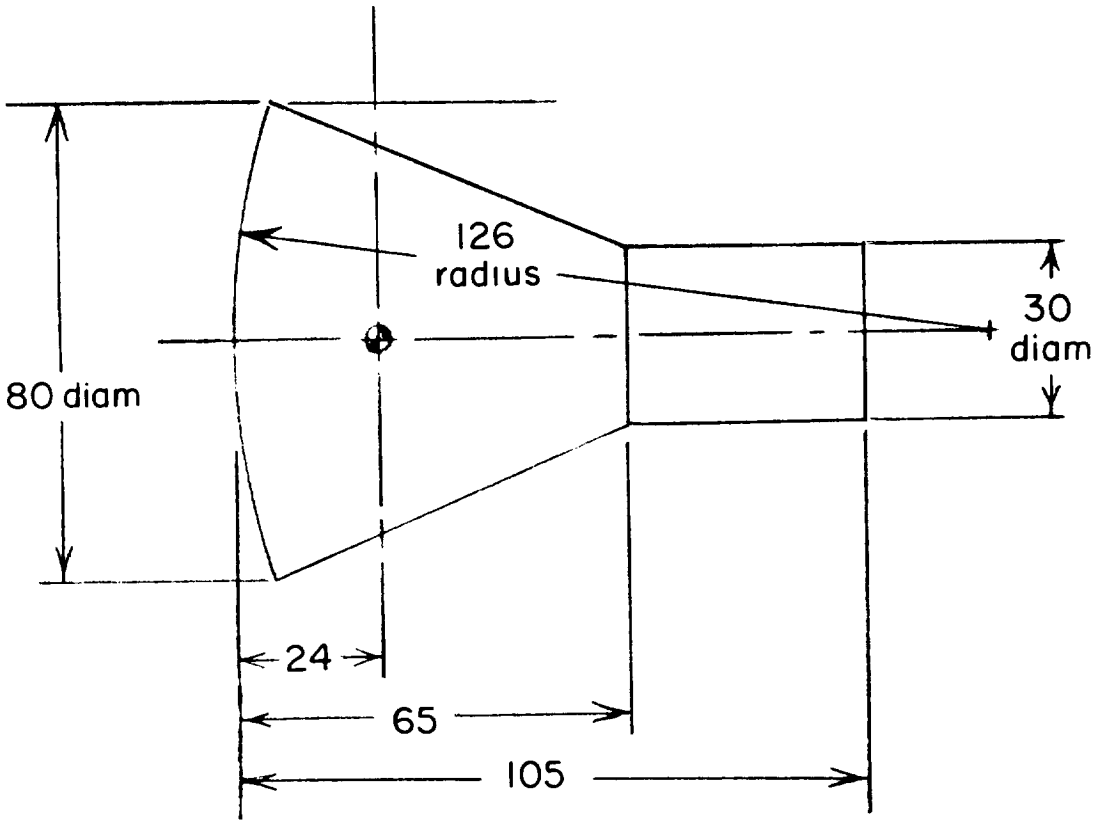

Figure 2.- Configuration approximately representative of that for which the computations were made. Dimensions are in inches.

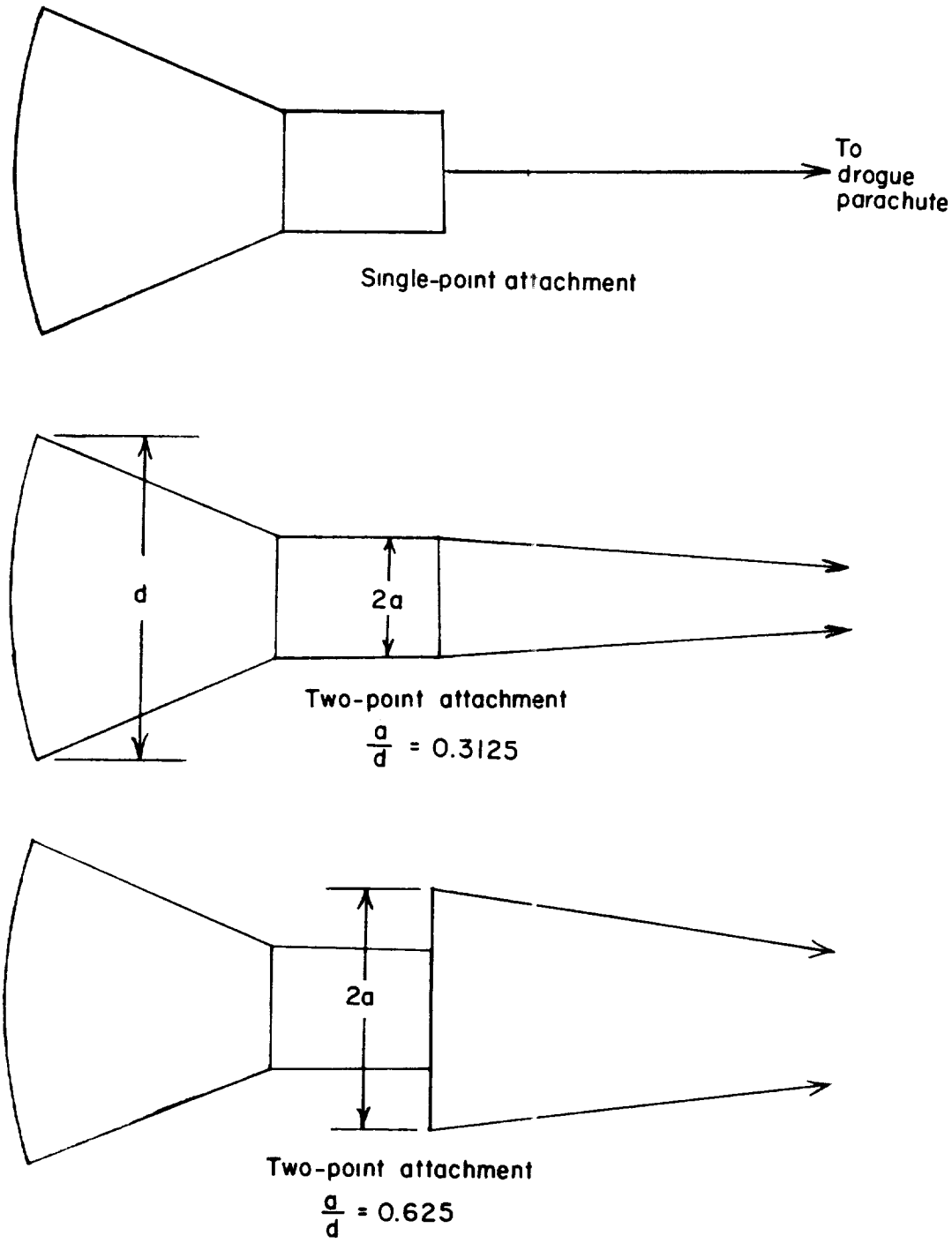

Figure 3.- Sketch showing the various drogue-parachute-attachment methods considered.

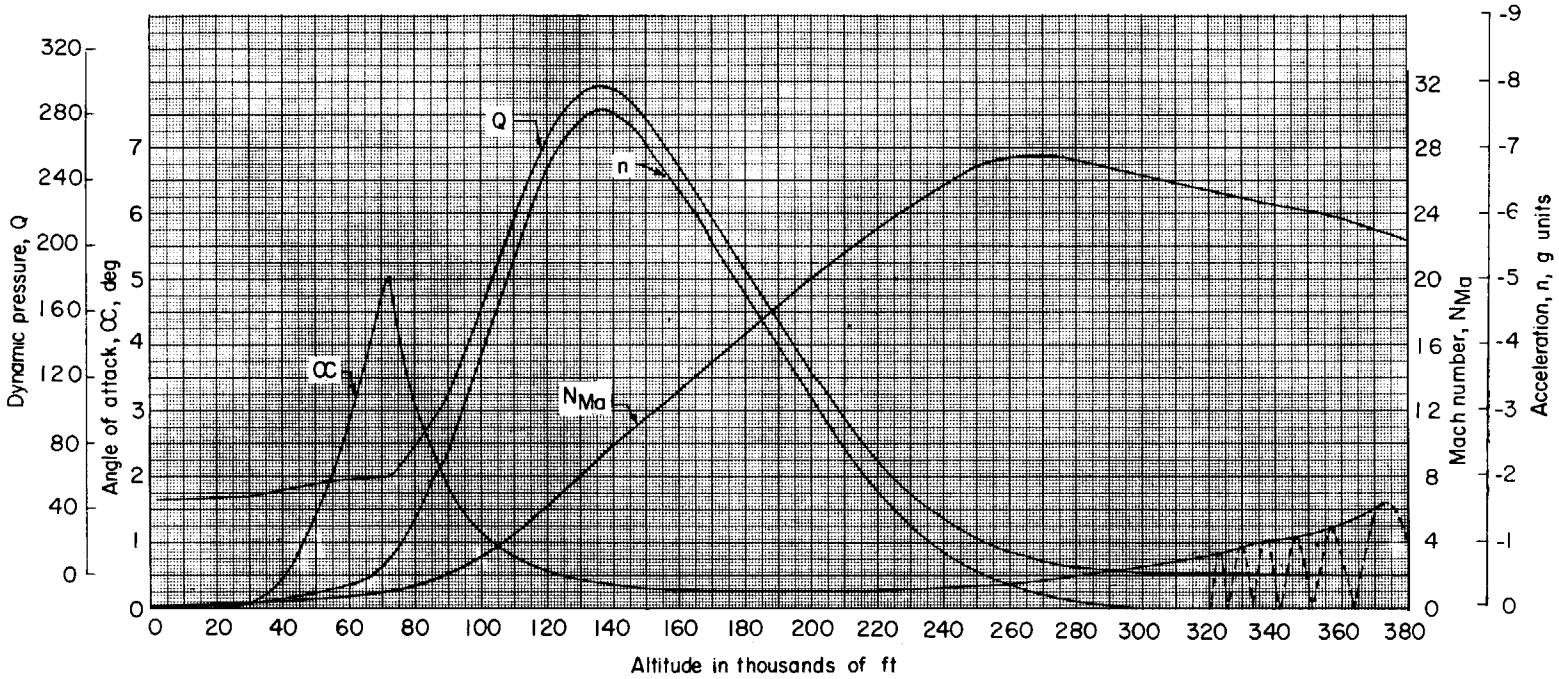

(a) Variation of α envelope, N_{Ma}, Q, and n with altitude.

Figure 4.- For the basic condition, variation of angle-of-attack envelope, Mach number, dynamic pressure, and acceleration along the flight path with altitude, and variation of altitude with range trajectory.

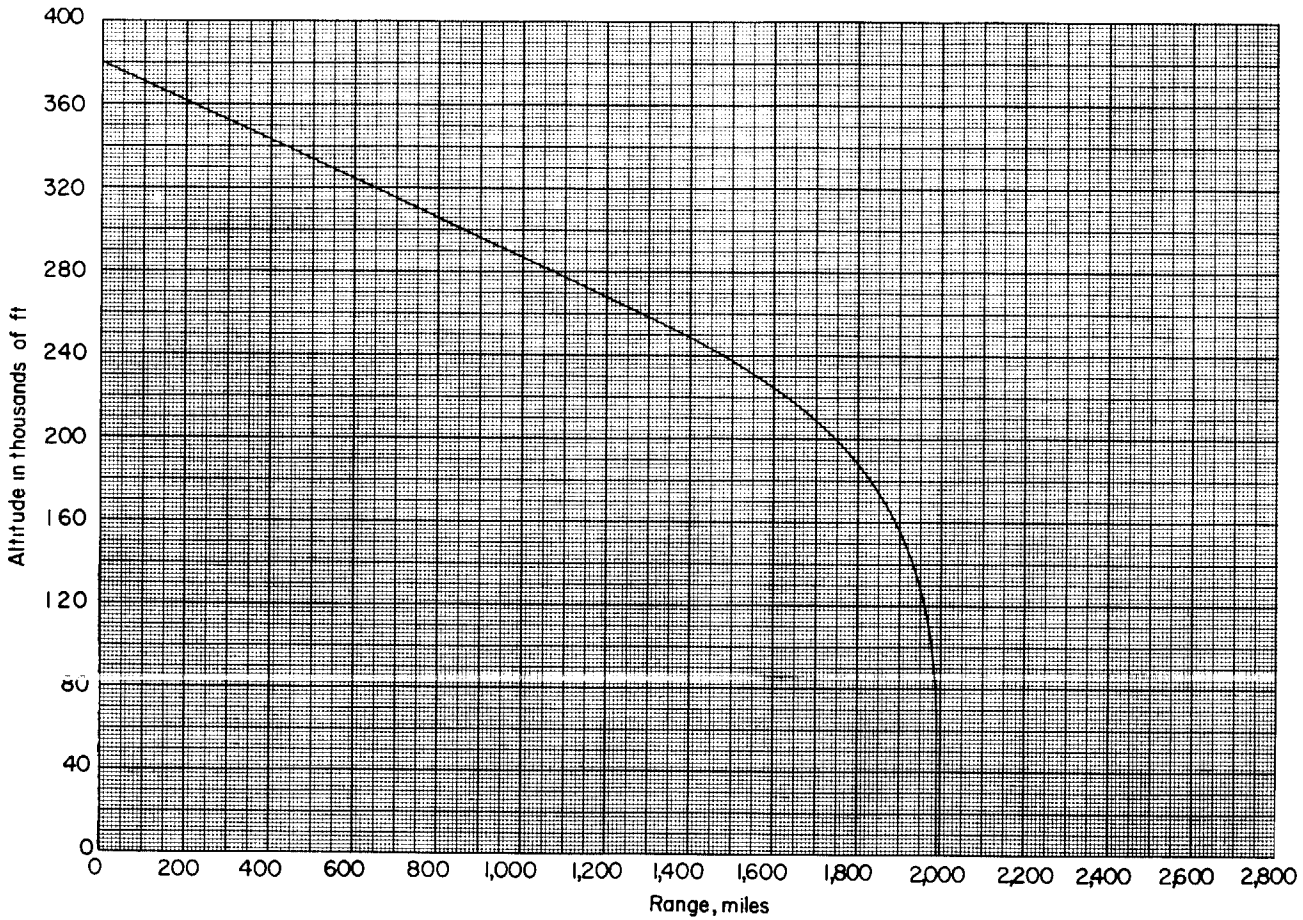

(b) Trajectory.

Figure 4.- Concluded.

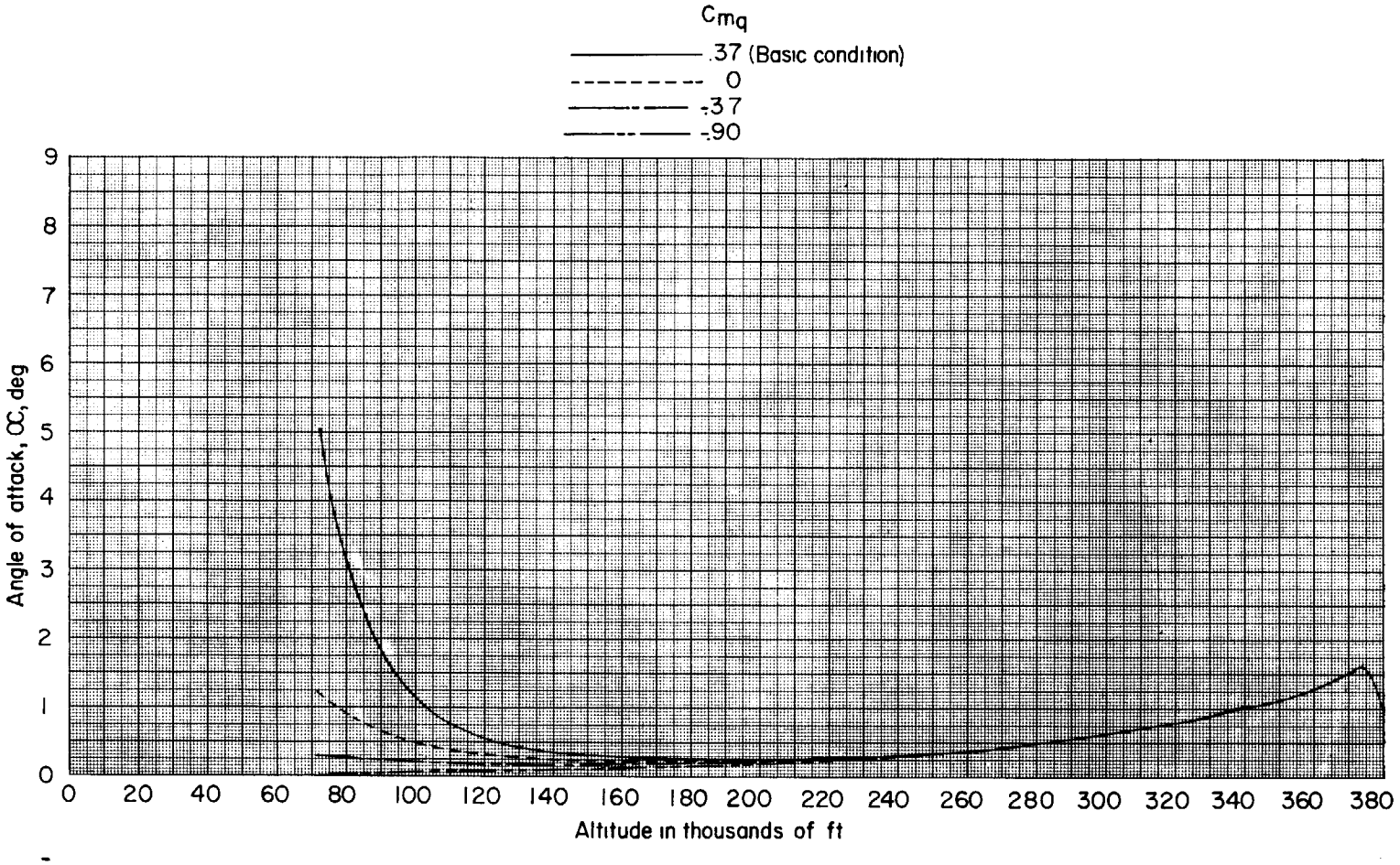

(a) Effect of C_{m_q}.

Figure 5.- Effect of aerodynamic derivatives on angle-of-attack envelope.

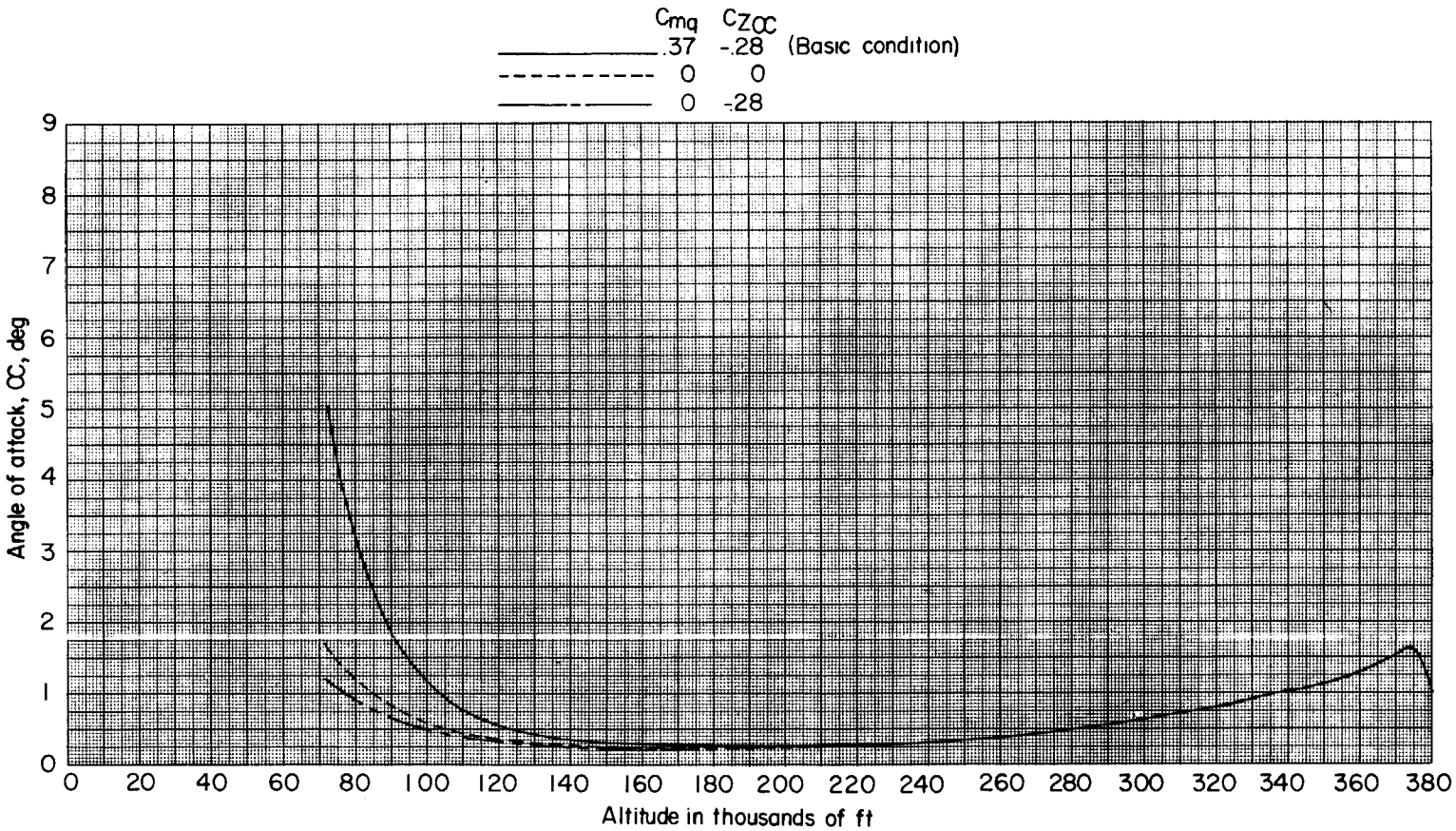

(b) Effect of C_{Z_α}.

Figure 5.- Continued.

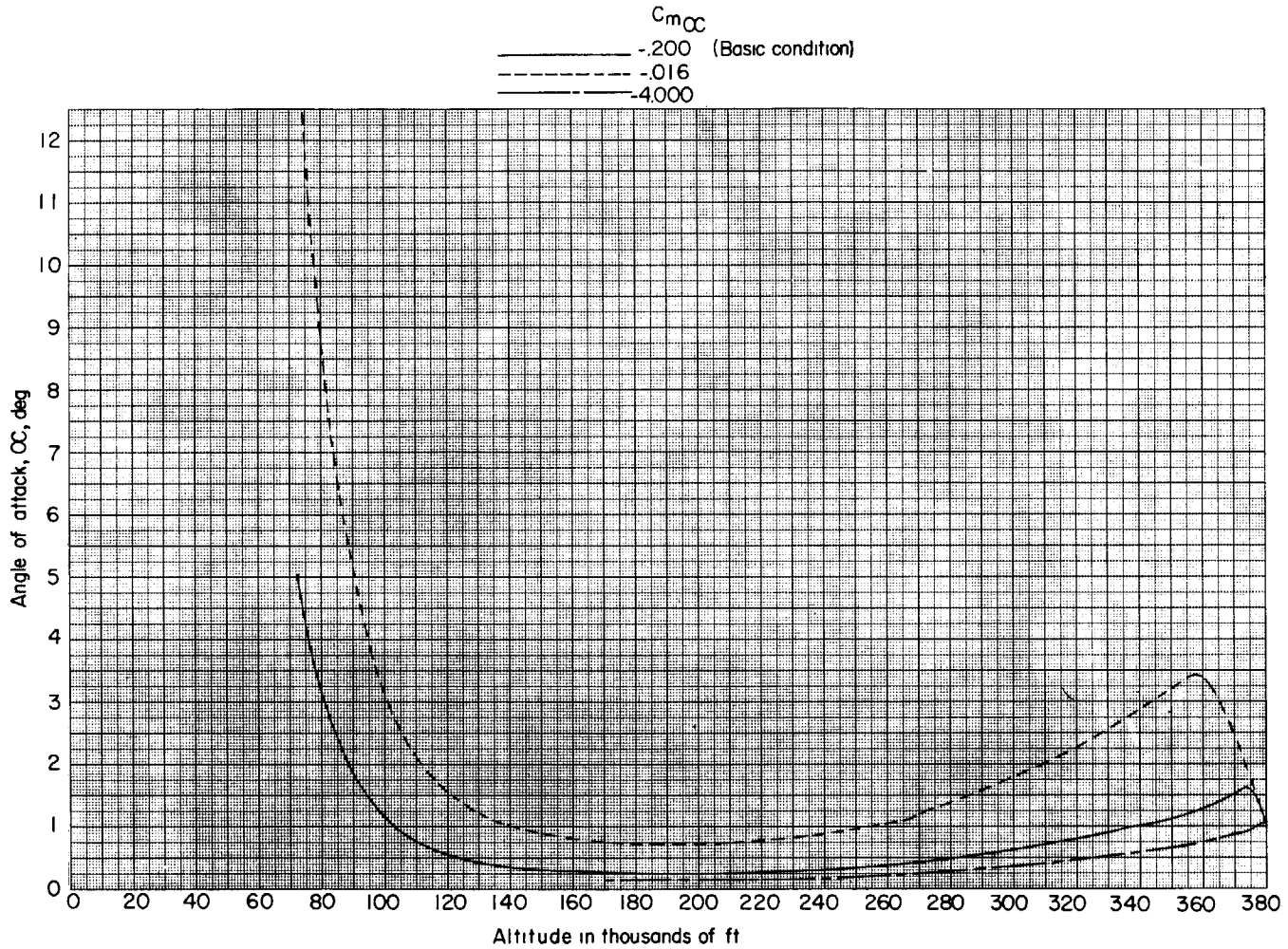

(c) Effect of $C_{m_{\alpha}}$.

Figure 5.- Concluded.

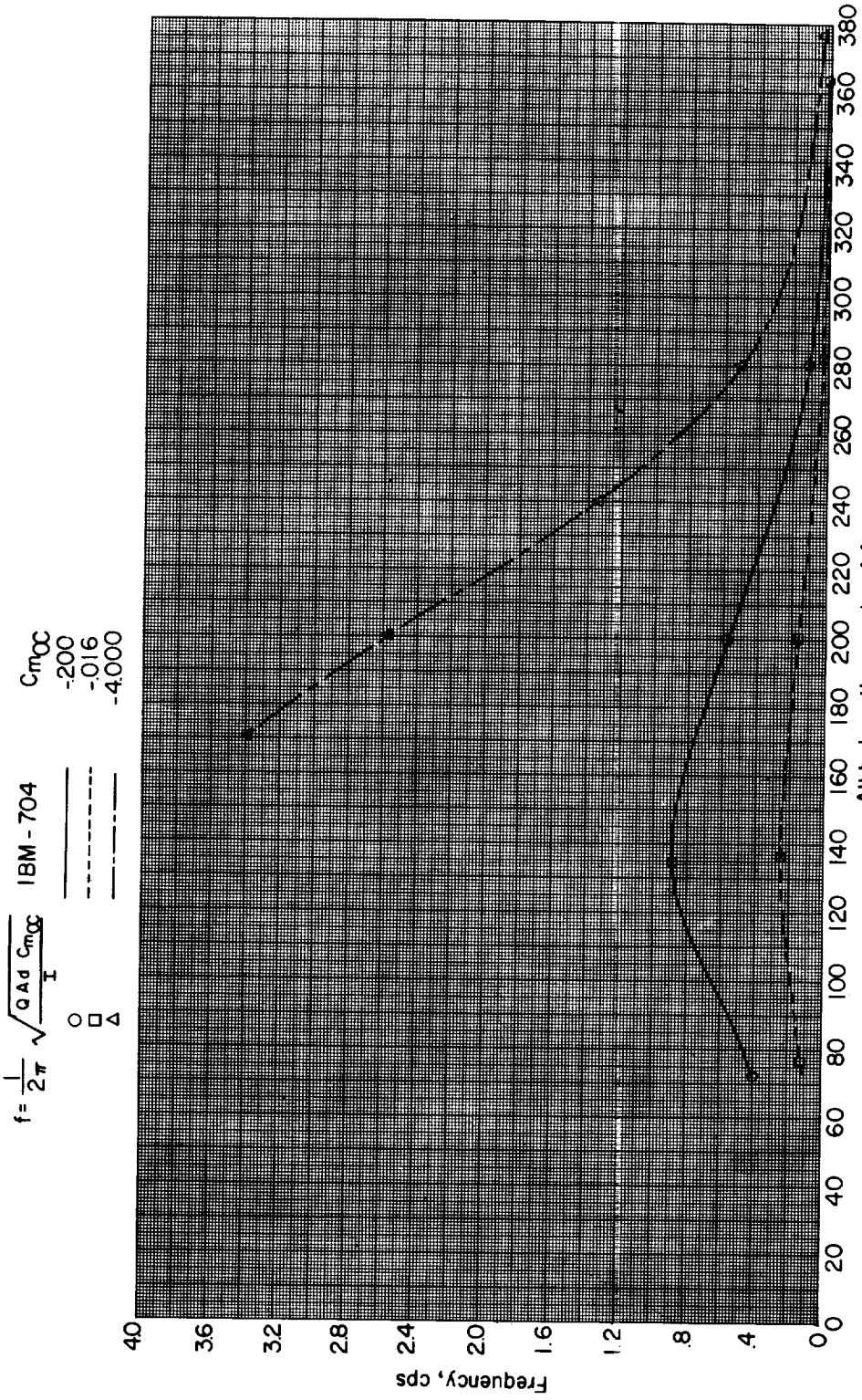

Figure 6.- Variation of computed frequency of oscillation with altitude.

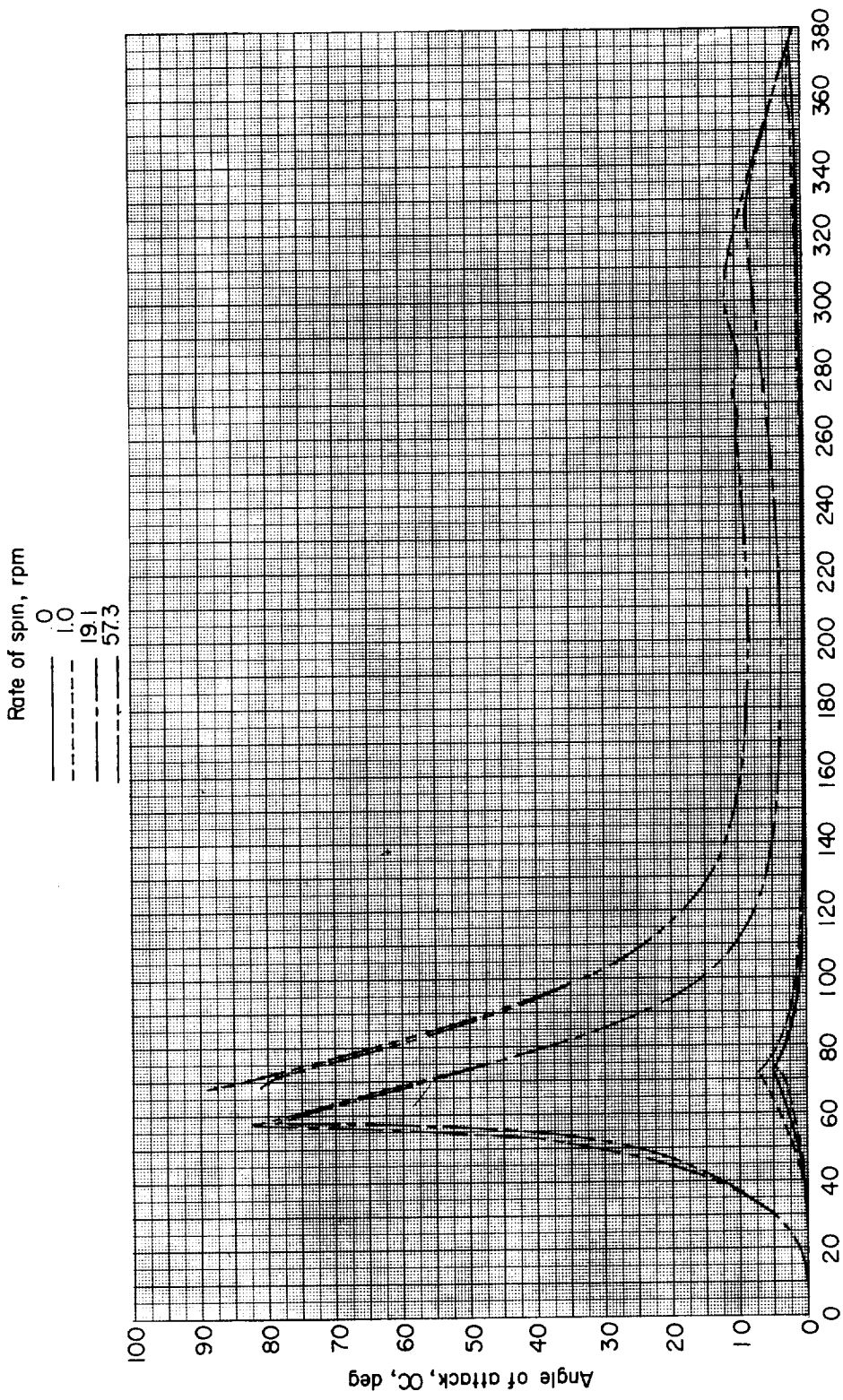

Figure 7.- Effect of rate of spin on angle-of-attack envelope. Double lines indicate maximum and minimum angles of attack.

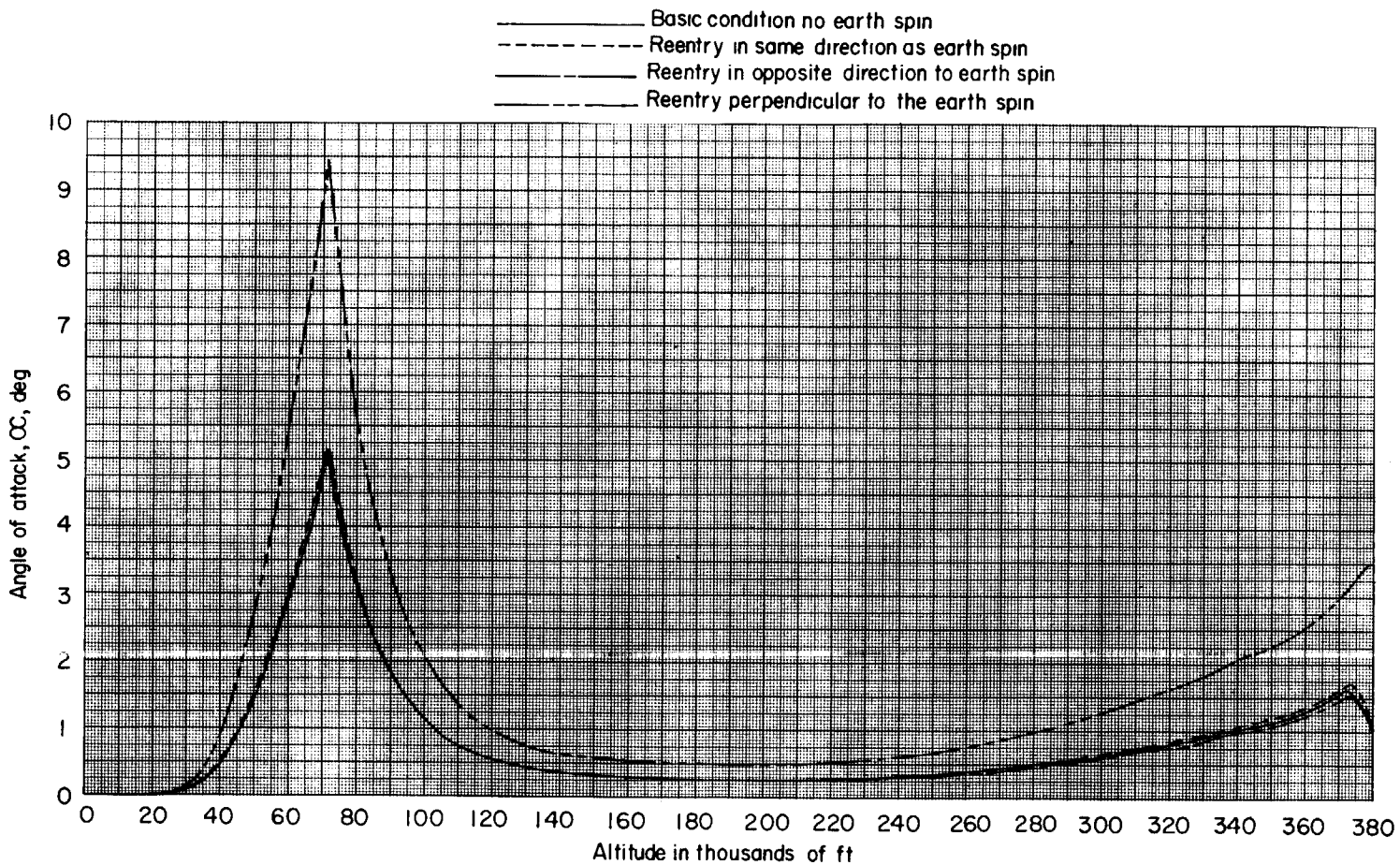

(a) Effect of geostrophic wind on angle-of-attack envelope.

Figure 8.- Effect of geostrophic wind on angle-of-attack envelope and trajectory.

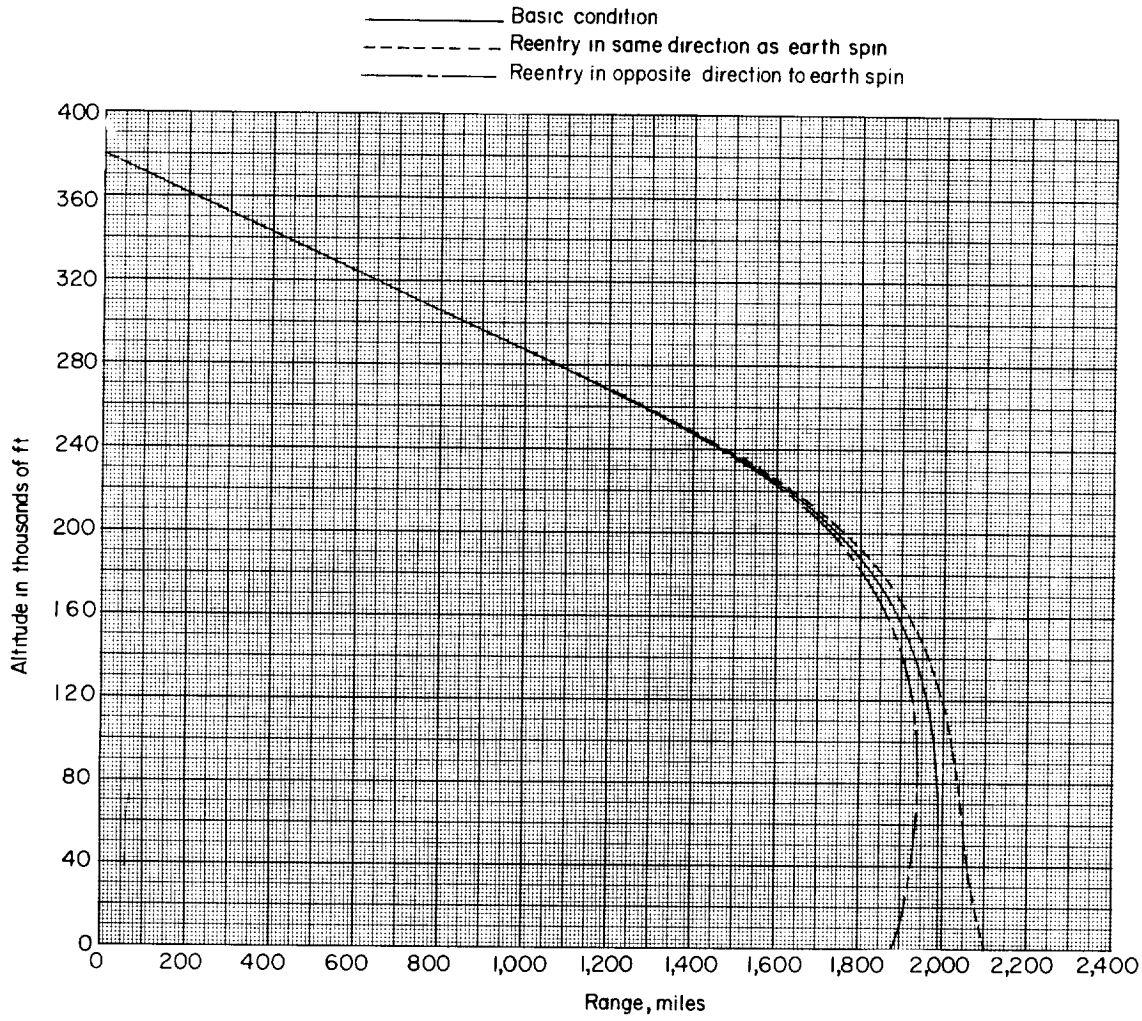

(b) Effect of geostrophic wind on range for head or tail winds.

Figure 8.- Continued.

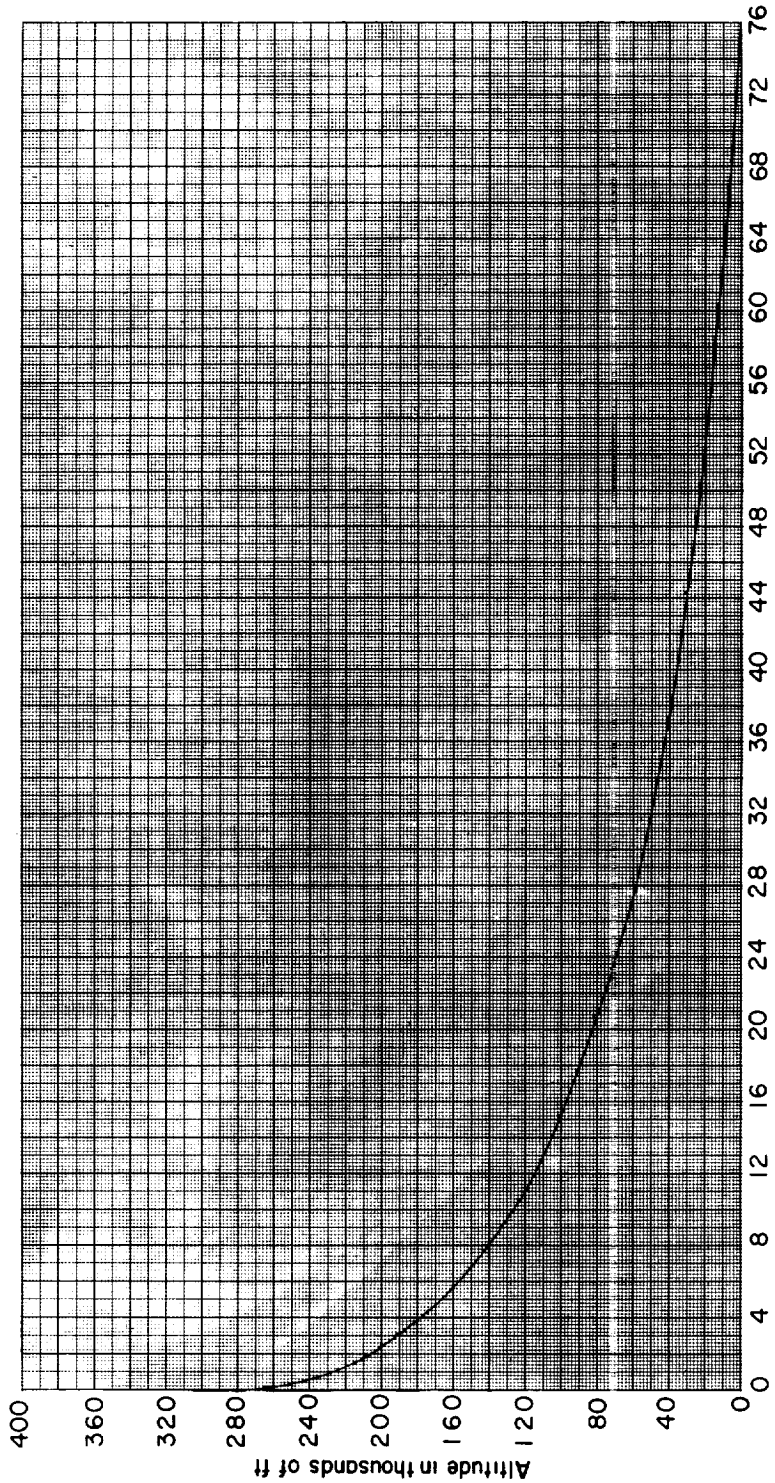

(c) Variation of sideward displacement with altitude for a north-south reentry.

Figure 8.- Concluded.

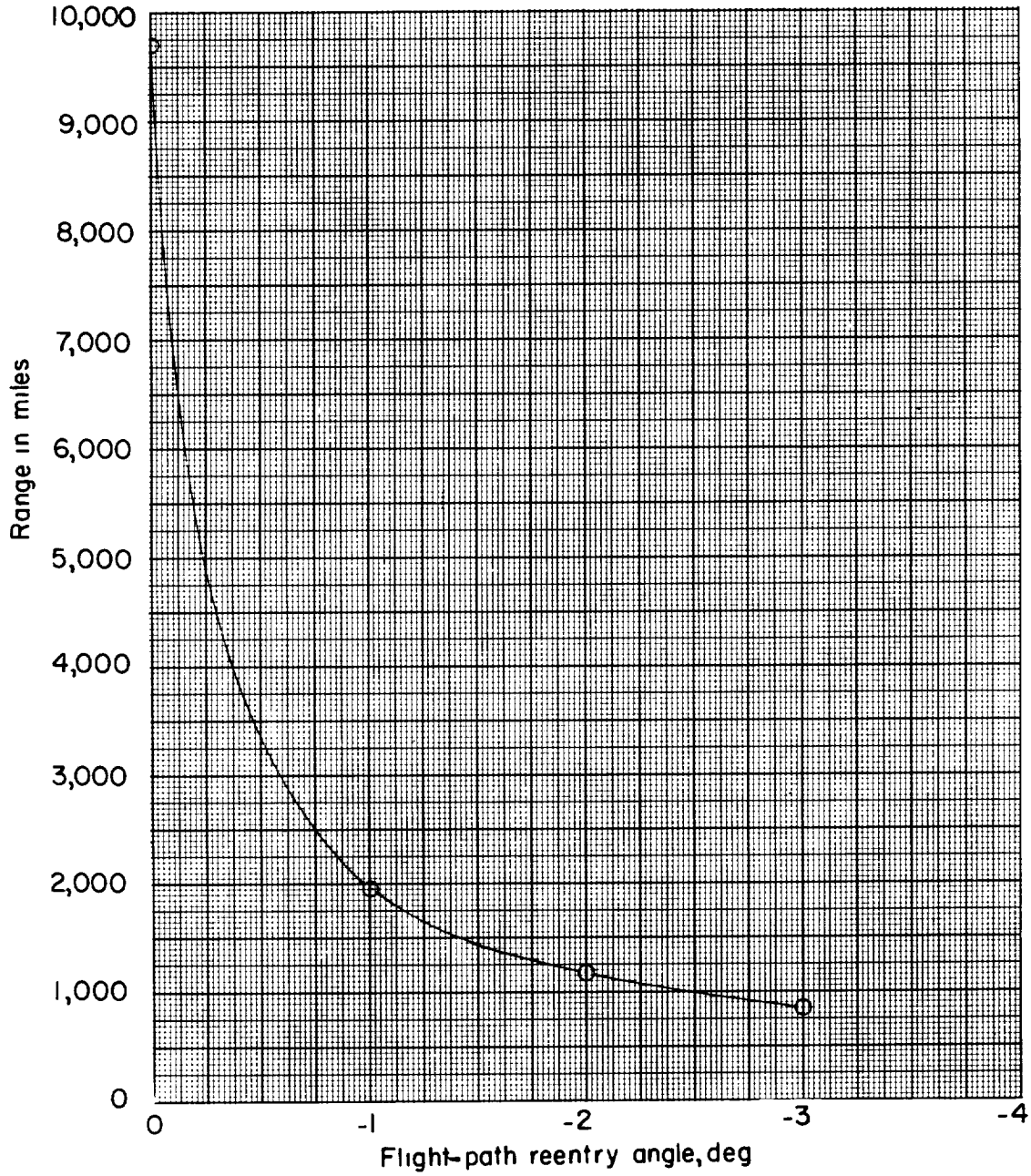

(a) Variation of range with angle of declination of reentry.

Figure 9.- Effect of initial declination of flight path on range trajectory and angle-of-attack envelope for orbital initial velocities. $\alpha_o = 1^o$.

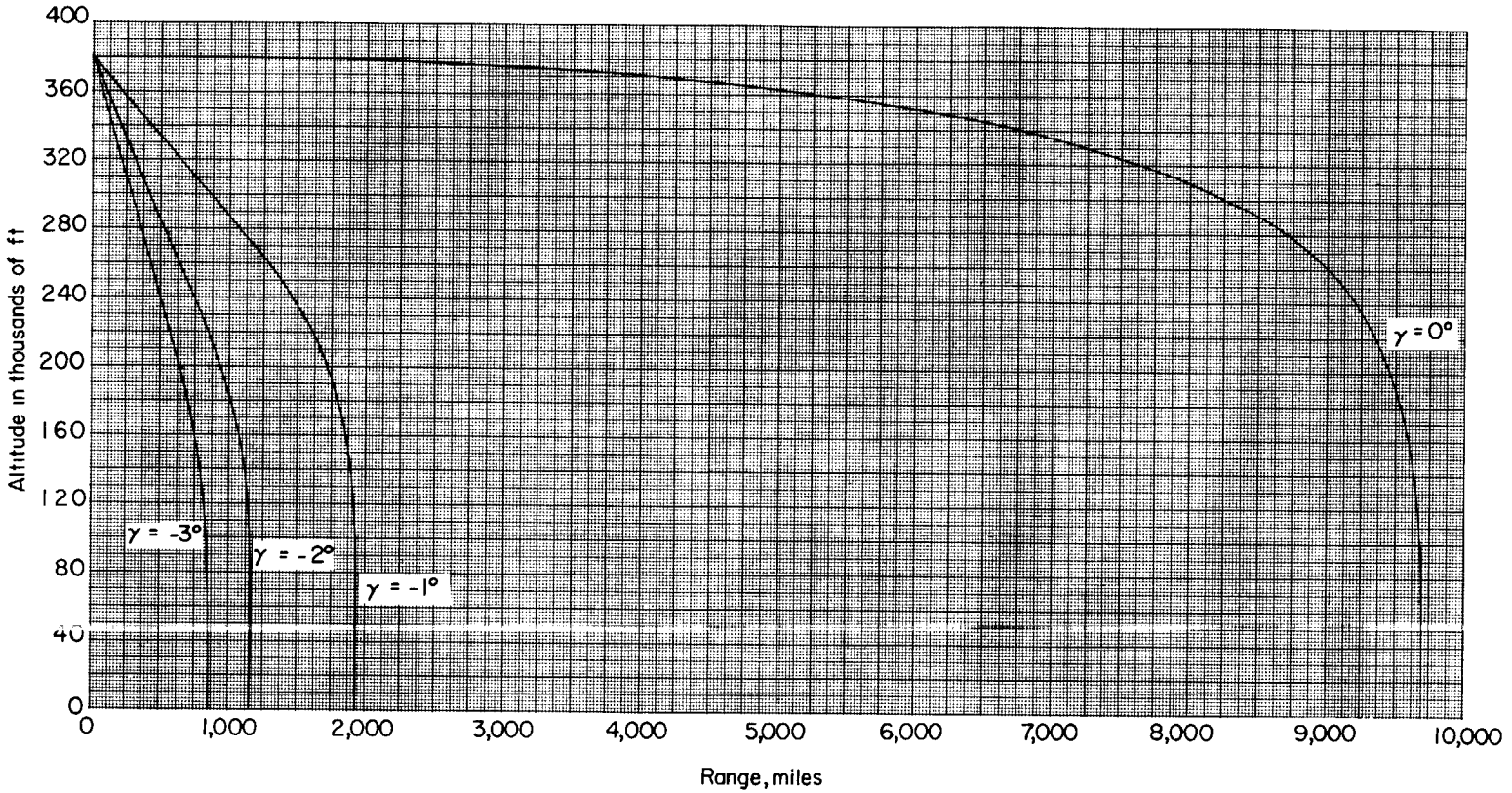

(b) Trajectories for various reentry angles.

Figure 9.- Continued.

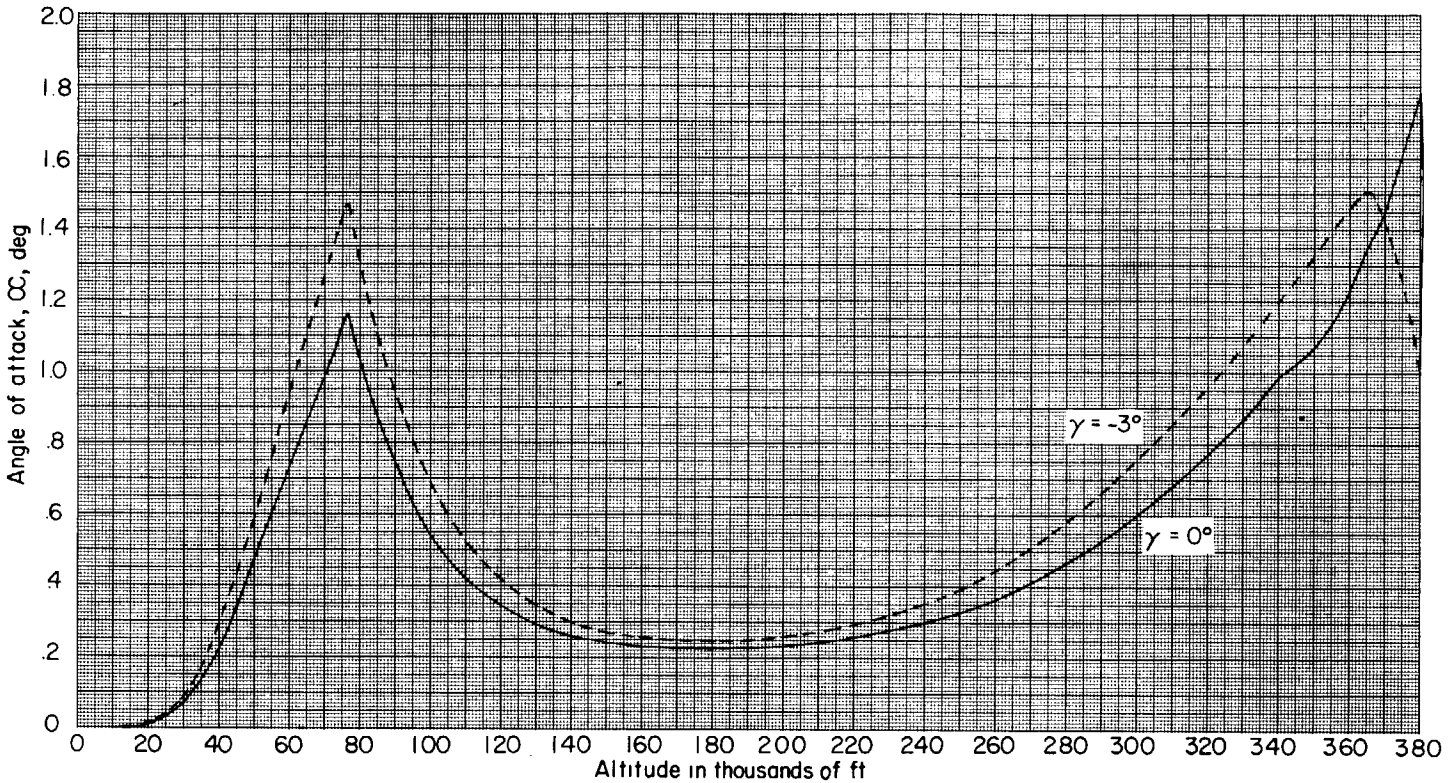

(c) Effect of reentry angle on angle-of-attack envelope.

Figure 9.- Concluded.

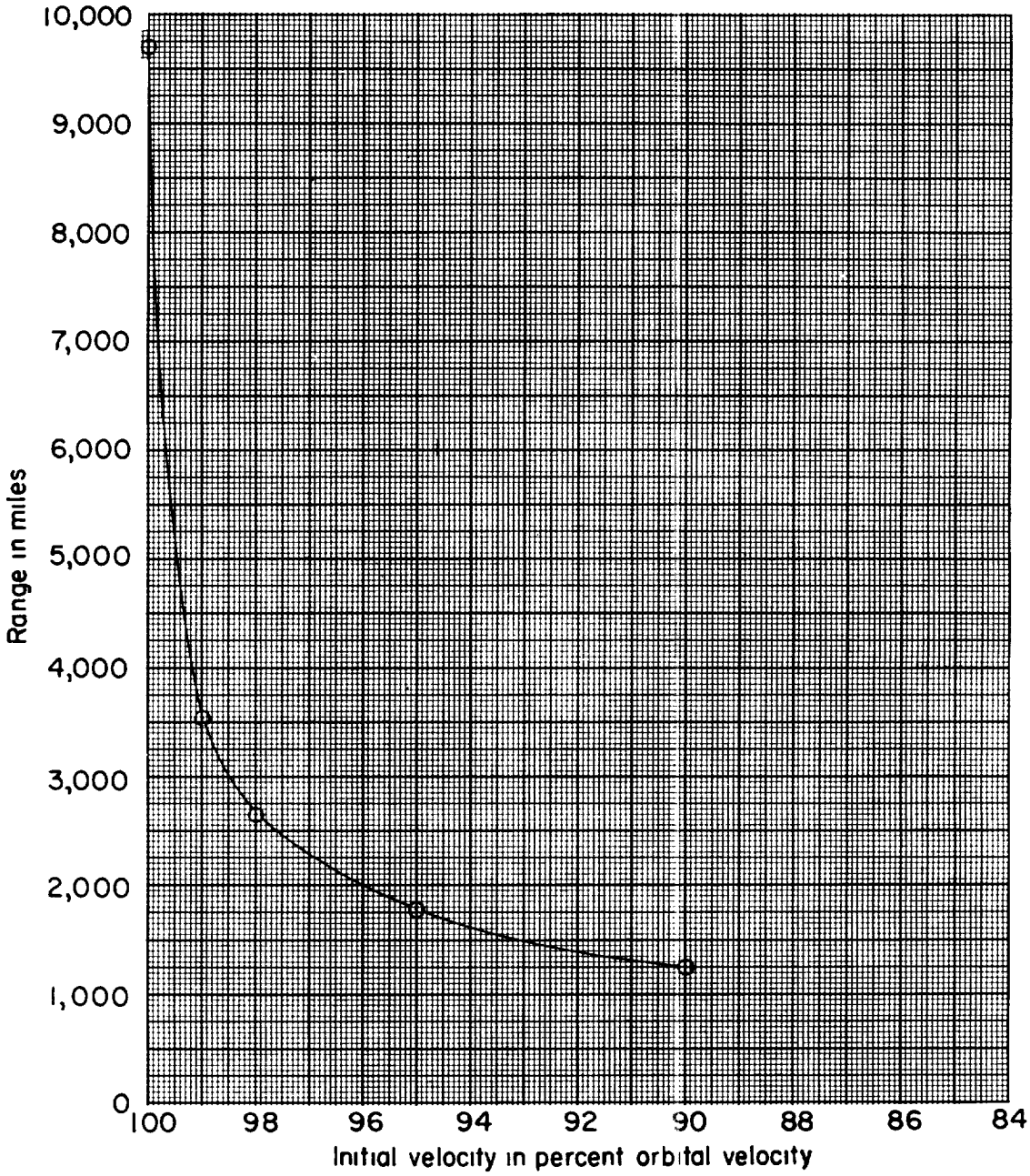

(a) Variation of range with initial velocity.

Figure 10.- Effect of change in initial velocity on range and angle-of-attack envelope for an entry angle of 0°. $\alpha_0 = 1^{\circ}$.

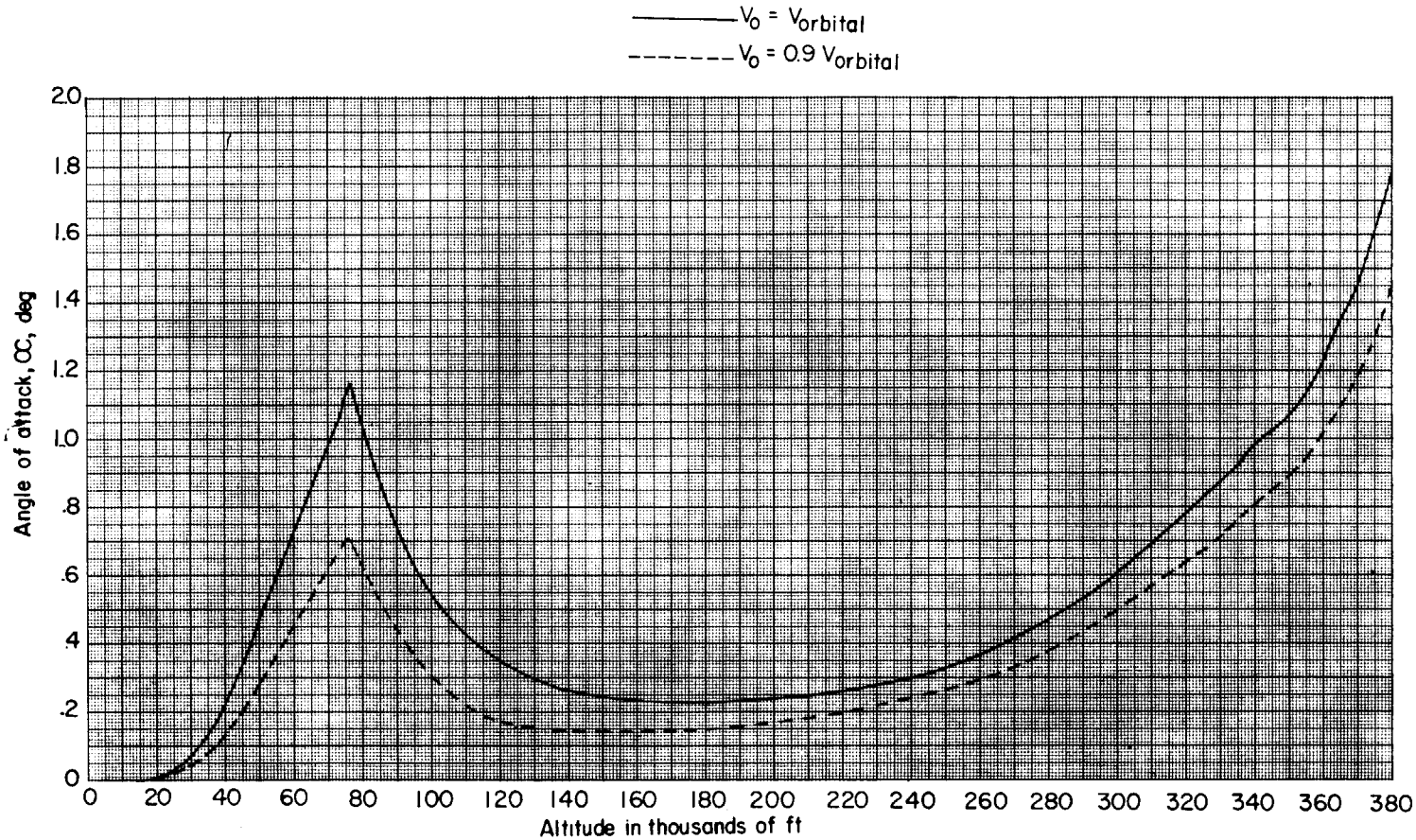

(b) Effect of initial velocity on angle-of-attack envelope.

Figure 10.- Concluded.

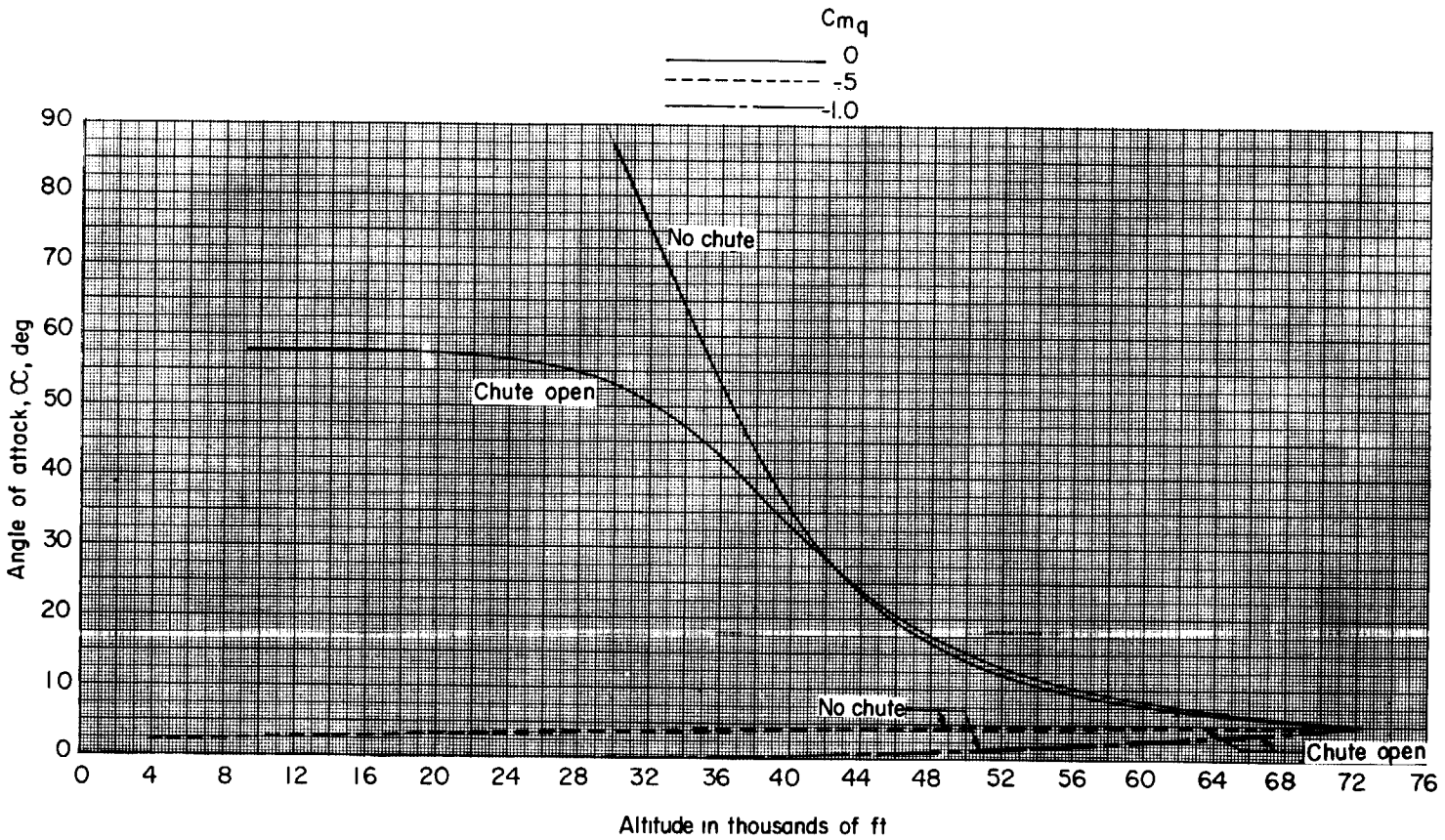

Figure 11.- Effect of C_{m_q} on angle-of-attack envelope below $N_{Ma} = 1$ without and with single-point-attachment drogue parachute.

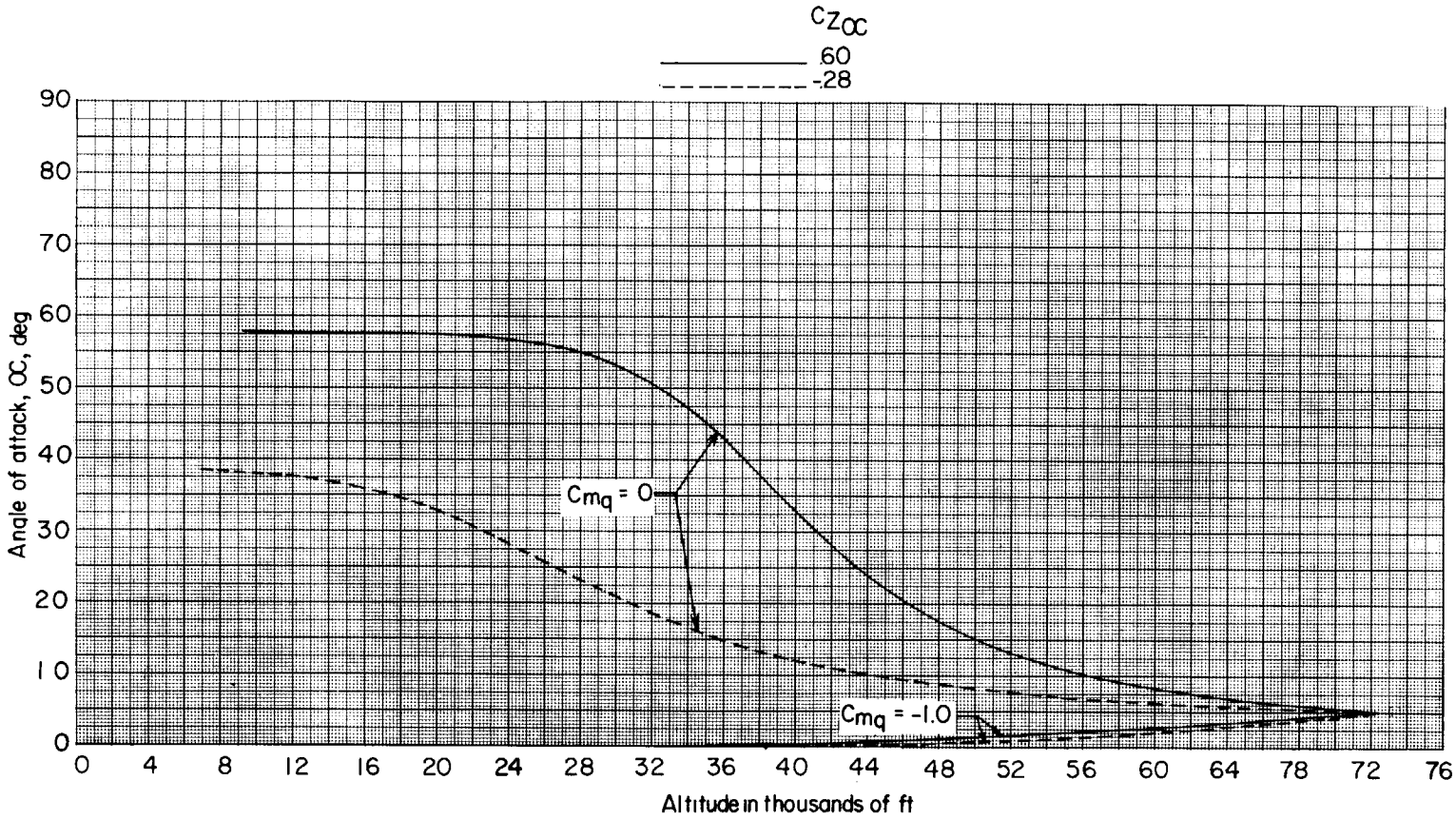

Figure 12.- Effect of $C_{Z_{\alpha}}$ on angle-of-attack envelope below $N_{Ma} = 1$ with the single-point-attachment drogue parachute.

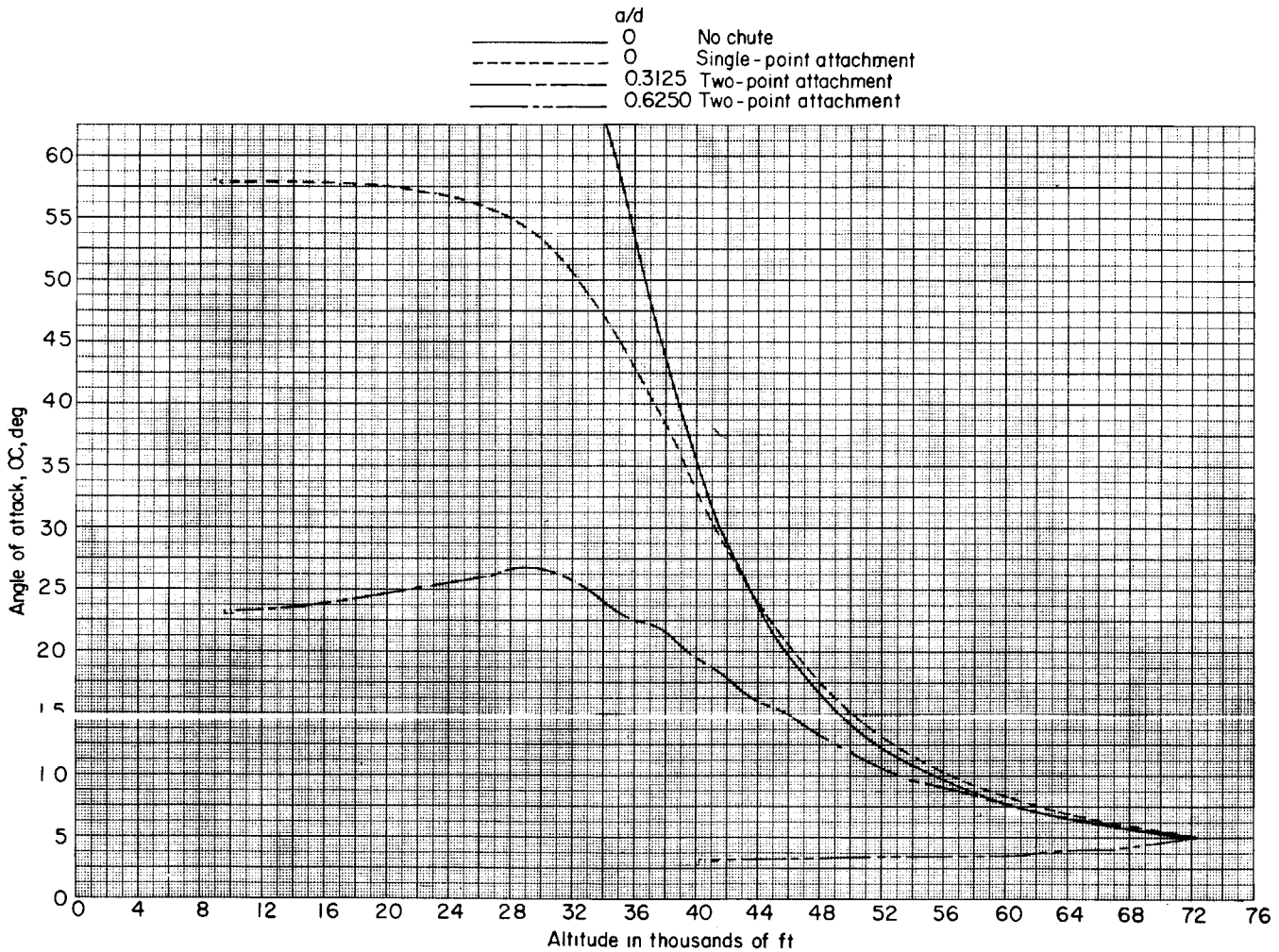

Figure 13.- Comparison of angle-of-attack envelopes for two-point and single-point parachute attachments with the envelope obtained when no drogue parachute is attached. $C_{m_q} = 0$.

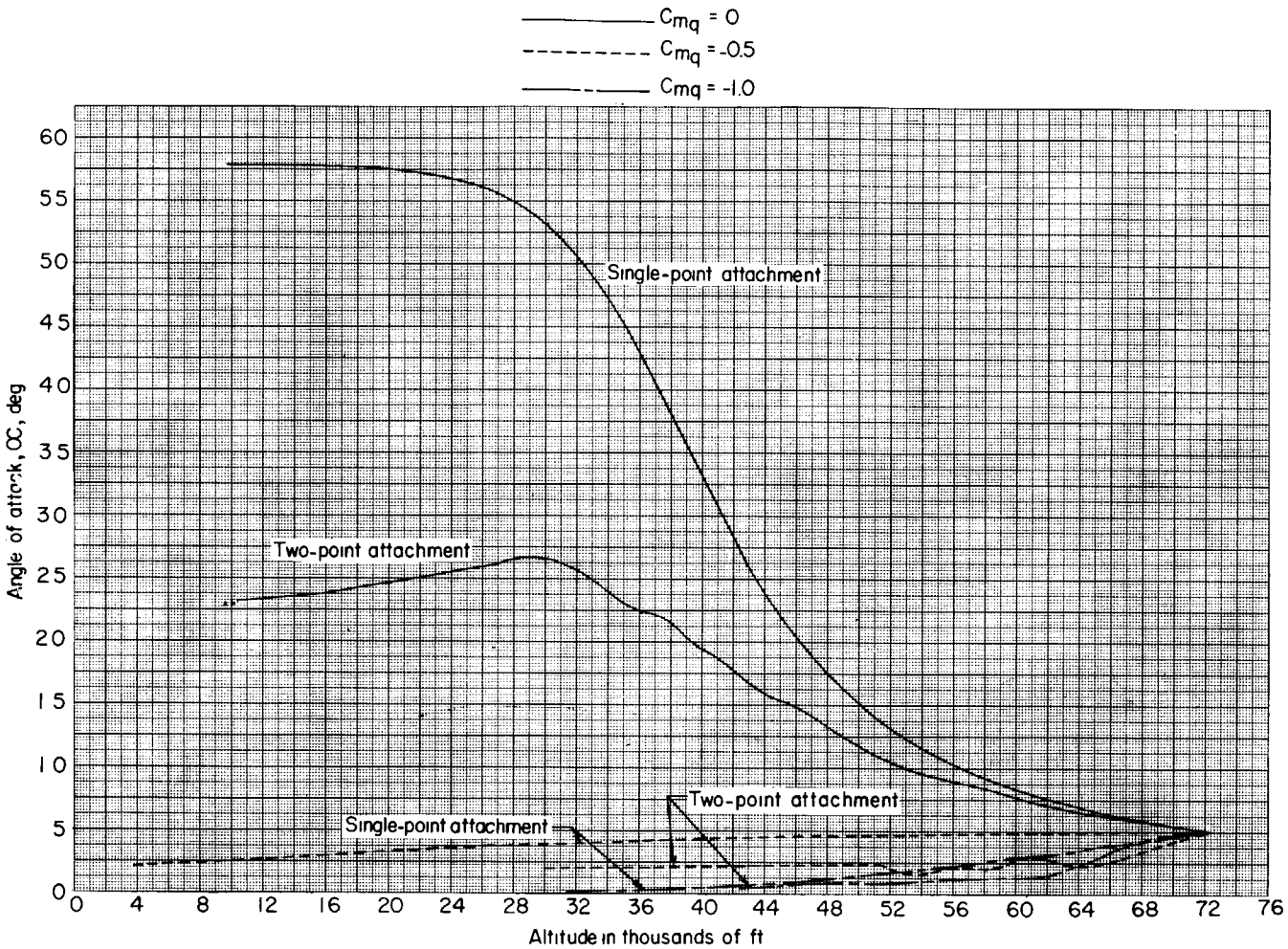

Figure 14.- Comparison of effect of C_{m_q} on angle-of-attack envelope for single- and two-point drogue-parachute attachment. a/d = 0.3125.

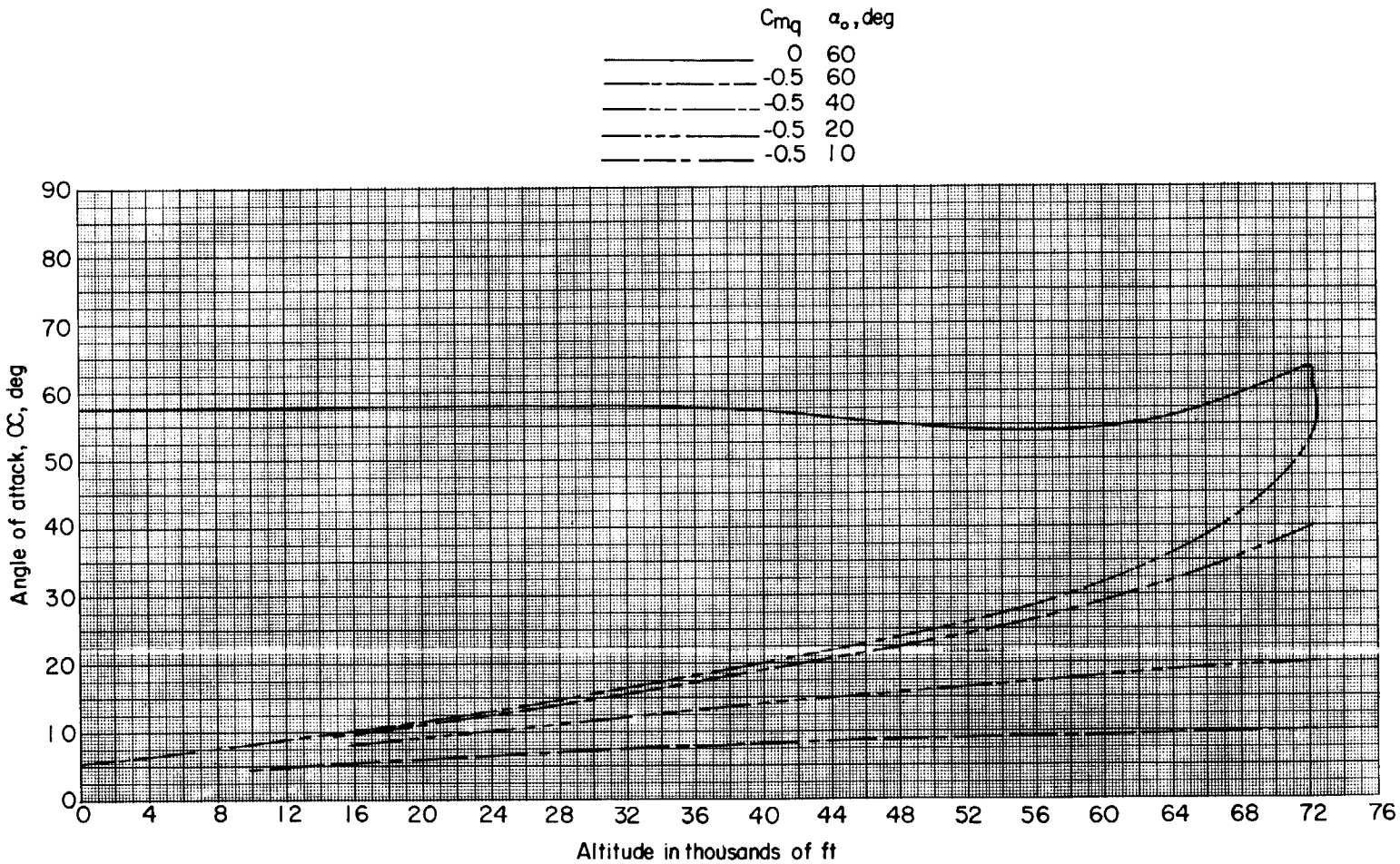

(a) Effect of single-point-attachment drogue parachute on angle-of-attack envelope.

Figure 15.- Effect of drogue-parachute damping at large initial angles of attack.

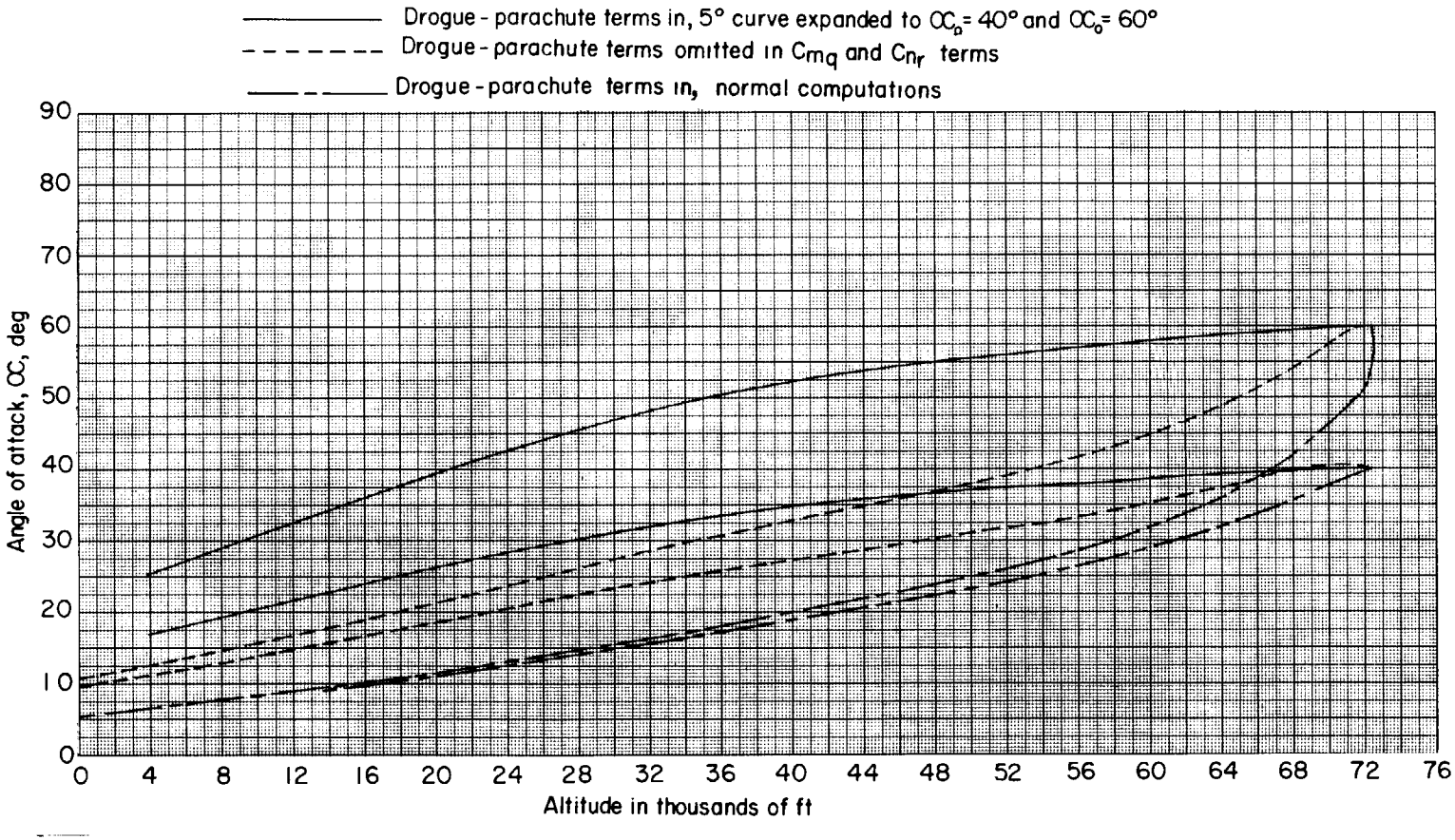

(b) Elaboration of drogue-parachute offset at large angle of attack. $C_{m_q} = -0.5$.

Figure 15.- Continued.

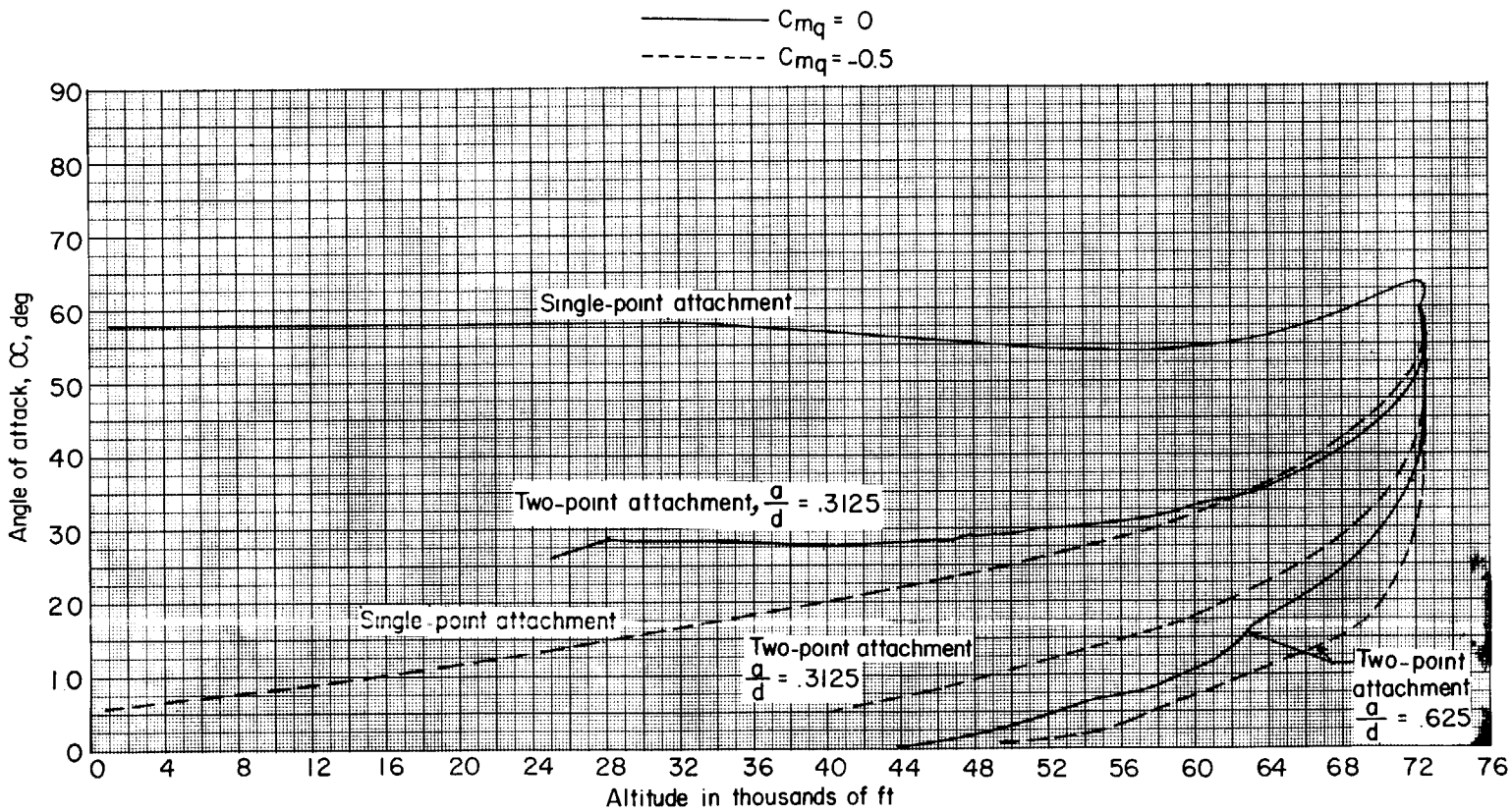

(c) Effect of drogue-parachute attachment on angle-of-attack envelope for initial amplitude of 60°.

Figure 15.- Continued.

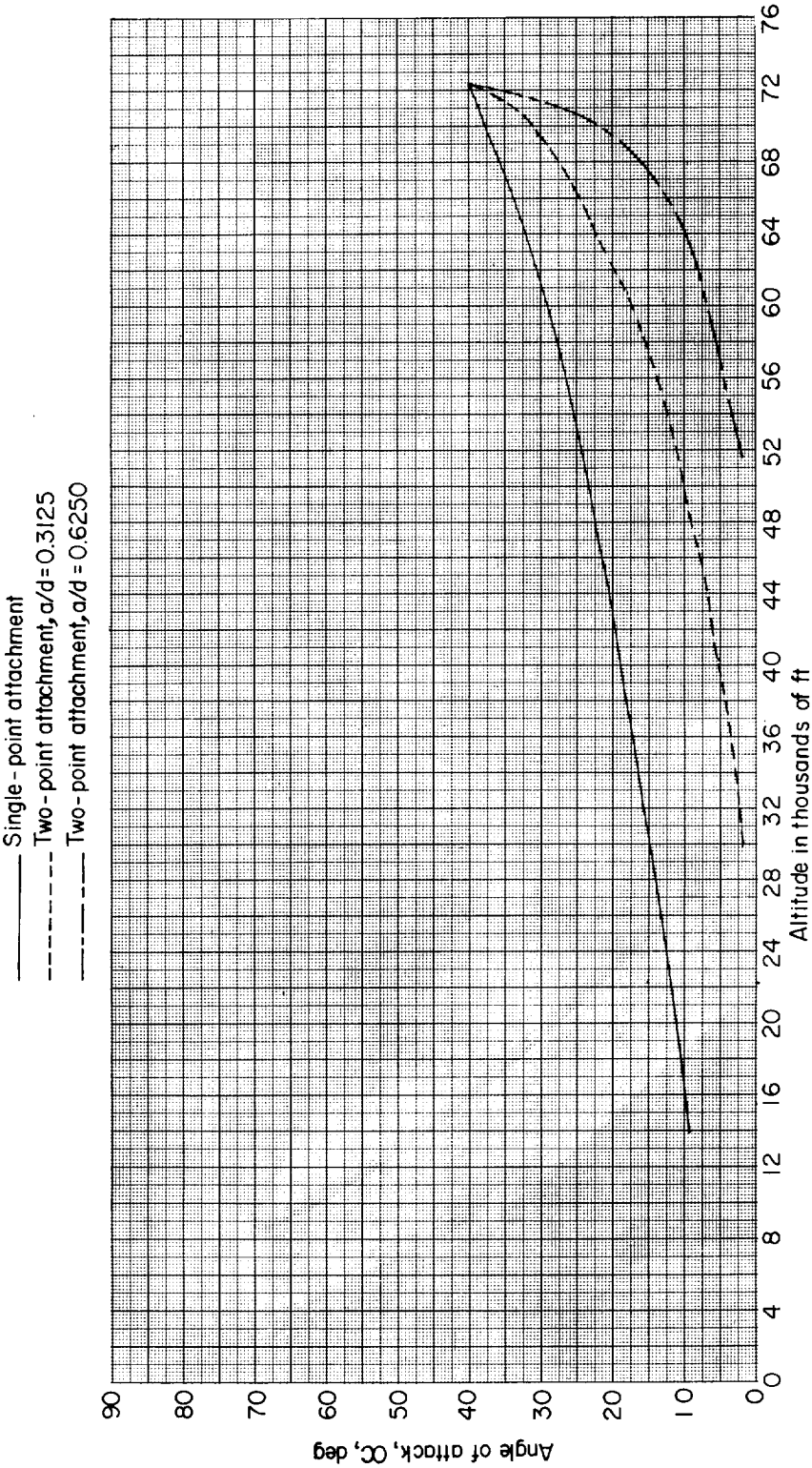

(d) Effect of drogue-parachute attachment on angle-of-attack envelope for initial amplitude of 40°. $C_{m_q} = -0.5$.

Figure 15.- Concluded.

NASA - Langley Field, Va. L-867